

The Möbius Domain Wall Fermion Algorithm

Richard C. Brower

Department of Physics, Boston University, 590 Commonwealth Avenue, Boston, MA
02215, USA

Harmut Neff

Chamerstrasse 44, 6300 Zug, Switzerland, email: hartmutneff@aol.com

Kostas Orginos

Department of Physics, College of William and Mary, Williamsburg, VA 23187-8795

Jefferson Laboratory, 12000 Jefferson Avenue, Newport News, VA 23606

November 6, 2014

Abstract

We present a review of the properties of generalized domain wall Fermions, based on a (real) Möbius transformation on the Wilson overlap kernel, discussing their algorithmic efficiency, the degree of explicit chiral violations measured by the residual mass (m_{res}) and the Ward-Takahashi identities. The Möbius class interpolates between Shamir's domain wall operator and Boriçi's domain wall implementation of Neuberger's overlap operator without increasing the number of Dirac applications per conjugate gradient iteration. A new scaling parameter (α) reduces chiral violations at finite fifth dimension (L_s) but yields exactly the same overlap action in the limit $L_s \rightarrow \infty$. Through the use of 4d Red/Black preconditioning and optimal tuning for the scaling $\alpha(L_s)$, we show that chiral symmetry violations are typically reduced by an order of magnitude at fixed L_s . At large L_s we argue that the observed scaling for $m_{res} = O(1/L_s)$ for Shamir is replaced by $m_{res} = O(1/L_s^2)$ for the properly tuned Möbius algorithm with $\alpha = O(L_s)$.

1 Introduction

Perhaps the most important theoretical development in lattice field theory at the end of the last century was the discovery of Fermion actions that respect exact chiral symmetry at finite lattice spacing. The consequence of this is a clean separation between chiral symmetry breaking (i.e. non-zero quark masses) and Lorentz breaking (i.e. non-zero lattice spacing). Even at finite lattice spacing, this allows for a rigorous understanding of topology and greatly simplifies the numerical extrapolations to obtain renormalized correlation functions in the continuum limit with the light quarks masses at their physical value.

The key idea in evading the Nielsen-Ninomiya no-go theorem [1, 2], which forbade the construction of lattice Fermion action with chiral symmetry under rather general conditions, was introduced by Kaplan [3]. In his construction four dimensional chiral zero modes appeared as bound states on a mass defect or 3-brane in a five dimensional theory. Much like the work of Callan and Harvey [4] in the continuum, anomalous currents in the 4 dimensional theory are understood as the flow on or off the mass defect of conserved 5 dimensional currents. This work led to two concrete realizations of lattice Fermions with chiral symmetry: the domain wall Fermions [5, 6] and the overlap Fermions [7, 8, 9, 10, 11]. The domain wall formulation retains the five dimensional nature of the original idea, while the overlap is a direct construction of a four dimensional effective action. It was subsequently realized, that the 4d effective Fermion operator, $D_{ov}(m)$, of the domain wall action also satisfies the so called Ginsparg-Wilson (GW) relation [12],

$$\gamma_5 D_{ov}^{-1}(0) + D_{ov}^{-1}(0) \gamma_5 = 2R \gamma_5 , \quad (1.1)$$

where $D_{ov}(0)$ is the massless Dirac operator and $R = O(a)$ is a local operator. Taking $R = 1$ in lattice units, a solution to the GW relation is $D_{ov}(0) = \frac{1}{2} + \frac{1}{2} \gamma_5 \epsilon [H_5]$ where H_5 is the Dirac Hamiltonian for the 5-th dimension. Clearly the on-shell zero mass Fermion action is chiral: $\{\gamma_5, D_{ov}^{-1}(0)\} \sim 0$. The Ginsparg-Wilson relation was discovered in the context of an exact renormalization group improved Fermion actions in the free field limit [12]. More than a decade later, it was realized [13], that the classical (or so called perfect action [14, 15]) approximation to the renormalization group for the Fermion actions in a fixed gauge background still satisfies the GW relation. The Ginsparg-Wilson relation implies a modified lattice form of infinitesimal chiral rotations and it can be viewed as an alternative explanation of how the conditions of the Nielsen-Ninomiya theorem are circumvented [16].

Ultimately the domain wall and overlap Fermions are equivalent, requiring numerical algorithms which implement an approximation to the GW relations. In the domain wall formu-

lation, this approximation is a consequence of the finite extent of the fifth dimension, $L_s < \infty$, whereas for the overlap algorithm a finite rational approximation to the sign function, $\epsilon_{L_s}[H_5]$. In both cases the resulting lattice actions have small chiral symmetry violations parameterized by the defect in the GW relation (see Eq. 2.5 below), which in principle can be reduced as needed to levels that do not seriously affect the physics.

The Möbius generalization for domain wall Fermions was introduced 7 years ago [17, 18] but is just now beginning to make its way into large scale simulations. Not only has this improvement not been fully exploited, there are new opportunities to leverage this algorithm with subsequent developments such as Gap Fermion [19] and as a preconditioner as, for example, in the MADWF algorithm [20] using Pochinsky’s MDWF inverter code [21] or multigrid methods [22, 23, 24]. Consequently it is timely to give a review of some of the basic formalism that leads to the Möbius generalization of domain wall Fermions. In addition, the Möbius generalization calls for a more careful arrangement of the standard analysis of domain wall Fermion properties. While very little of this formalism is entirely original [7, 8, 9, 10, 11, 25, 26, 27, 28, 17, 18, 29, 30], we seek to abstract the basic structure of the domain wall operators and its equivalence to Overlap in a higher level framework so that the Möbius class of generalized domain wall operator is only visible at the level of implementation much in the spirit of object oriented software practices. Consequently we will define precisely the mapping between the 5d domain wall action and the effective 4d Overlap operator at fixed L_s , including the general way to formulate residual chiral breaking for correlators and the Ward-Takahashi identities.

The Möbius generalization introduces two new parameters in the domain wall fermion action. One parameter controls the kernel of the resulting Overlap operator allowing for a continuous family of kernels that have the Neuberger [10, 11] and the Shamir kernels [5] as special cases. The other is a scaling parameter α for the kernel that drops out of the 4D action in the $L_s \rightarrow \infty$ limit, providing a better approximation to the GW relation at finite L_s . In this sense it is proper to consider the scaling parameter α as offering a better **algorithm** for the same operator. For finite L_s the result is that the Möbius generalization offers a very substantial algorithmic advantage at fixed residual mass, particularly at large L_s . For example in current practice to get a sufficiently small residual mass for thermodynamics [31] and $\mathcal{N} = 1$ SUSY [32] the Shamir algorithm with a fifth dimension as large as $L_s = 48$ has been used. Here a rescaled Möbius gives to reasonably high accuracy an equivalent action by rescaling to $L_s = 12 - 16$ or a rescaling parameter $\alpha = 3 - 4$. By reducing the extent of the 5th dimension, the Dirac solver should be accelerated by roughly this factor α in these applications. Empirical results are presented here to support this estimate. In addition, it is even possible to further reduce L_s at fixed m_{res} , as noted in the conclusion (see Figs.10 and 11), by combining the Möbius

algorithm with Gap method [19]. Consequently the Möbius algorithm can very substantially accelerate inverters in analysis and evolution code with speed up depending on the degree of chiral symmetry sought.

Finally we recognize interest in combining algorithms based on the equivalence of overlap and domain wall formalisms, since each may be optimal at different stages of a single Monte Carlo calculation. To accomplish this one needs to establish a precise equivalence between the domain wall and overlap formulations at finite lattice spacing and finite separation L_s of the domain walls. Here we extend to the Möbius implementation the exact mapping between the domain wall and overlap Fermion correlators ,

$$\langle \mathcal{O}[q, \bar{q}] \rangle_{DW} = \langle \mathcal{O}[\psi, \bar{\psi}] \rangle_{ov} . \quad (1.2)$$

We refer to this mapping as the **DW/Overlap Correspondence**. Of course for the Shamir action this mapping has been dealt with extensively in the literature [7, 8, 9, 10, 11, 25, 26, 27, 28]. Also we take the opportunity to develop a consistent notation for this correspondence, extending it to vector and axial currents and their Ward-Takahashi identities. By studying this for finite L_s , we identify in both domain wall and overlap formulation the consequence of violating chiral invariance due to approximations (at finite L_s) that result in an imperfect realization of the Ginsparg-Wilson identity. The correspondence is based on the descent relations of Callan and Harvey [4] that motivated Kaplan's original idea. In the 5d space there are only vector currents since 4d parity becomes a reflection of the 5-th direction. The symmetric and anti-symmetric projections in the 5-th direction for the 5d vector current become the effective 4d vector and axial currents respectively of the effective overlap action.

In this paper we separate the general analysis from the specific details that depend on the choice of the (domain wall, overlap) action and its approximation algorithms (using for example rational polynomial approximation, domain wall, etc.). In Sec. 2 we begin by a general statement of the choice of actions and the impact on an approximation to the Ginsparg-Wilson condition for chiral Fermions. Following this is the specific domain wall action for the Möbius Fermion generalization. Sec. 3 explains the necessity of a 4d Red Black preconditioning for the Möbius Fermion which is as effective as the 5d Red Black scheme used for the Shamir variant. In Sec. 4 we present the results from detailed numerical tests demonstrating the effectiveness of our formulation in reducing the cost of implementing domain wall Fermions. Sec. 5 presents the general mapping between a domain wall action and the overlap action that proves their equivalence at finite lattice spacing and given rational approximation. The map is applied to construction of the 4d vector and axial vector currents from the 5d vector domain wall current. In Sec. 6 we apply the equivalence formalism to establish the Ward-Takahashi identities for

vector and axial current operators as well as derive the axial and vector currents for Möbius Fermions. In addition, in this section we construct from the axial ward identity the residual mass as a measure of the violation of chiral symmetry due to finite L_s approximation to the overlap operator and related it to the violation of the Ginsparg-Wilson relation.

2 Möbius Domain Wall Fermions

Domain wall and overlap Fermions may be viewed as two alternative algorithms for generating chiral Fermions that satisfy the Ginsparg-Wilson relation. This mapping between domain wall and overlap Fermions is even useful when chirality is approximated by domain wall Fermions with finite separation between the walls in the 5th axis. Throughout this review, we shall emphasize this equivalence by identifying the effective 4d overlap operator,

$$D_{ov}^{(L_s)}(m) = \frac{1+m}{2} + \frac{1-m}{2} \gamma_5 \epsilon_{L_s} [\gamma_5 D^{kernel}(M_5)] , \quad (2.1)$$

resulting from the corresponding domain wall implementation at finite extent L_s for the 5th dimension. Strictly speaking we should always designate this approximation to the overlap operator by $D_{ov}^{(L_s)}(m)$ but to simplify the notation we leave this dependence on L_s implicit throughout. The class of suitable overlap operators is quite large, dictated by the choice of the 4d kernel, $D^{kernel}(M_5)$, and a particular algorithm to approximate the sign function: $\epsilon_L[x] \simeq \epsilon[x] = x/|x|$. For example the standard domain wall implementation gives the polar approximation [33, 26, 34] to the sign function (see Fig. 8) ,

$$\epsilon_{L_s}[H_5] = \frac{(1+H_5)^{L_s} - (1-H_5)^{L_s}}{(1+H_5)^{L_s} + (1-H_5)^{L_s}} , \quad (2.2)$$

where the 5th time “Hamiltonian” is $H_5 = \gamma_5 D^{kernel}(M_5)$ with transfer matrix $T = (1-H_5)/(1+H_5)$. There are many other ways to generate polynomial or rational polynomial approximations [35] to the sign function, some of which have a natural representation as a local action in the 5th time. The 5th time interpretation of Neuberger and Kaplan provide a very intuitive method to impose chiral symmetry, as we will see when discussing the axial current. Only in the limit $L_s \rightarrow \infty$, does the effective domain wall operator reproduce exactly Narayanan-Neuberger’s overlap Fermion [7, 8, 9].

The exact lattice chiral symmetry (at $m = 0$ and $L_s = \infty$) is guaranteed by the G-W relation,

$$\gamma_5 D_{ov}(0) + D_{ov}(0) \gamma_5 = 2 D_{ov}(0) \gamma_5 D_{ov}(0) . \quad (2.3)$$

We may recast G-W relations as, $\gamma_5 D_{ov}(0) + D_{ov}(0)\hat{\gamma}_5 = 0$, by introducing a new γ_5 operator,

$$\hat{\gamma}_5 = \gamma_5(1 - 2D_{ov}(0)) = -\epsilon[H_5], \quad (2.4)$$

which allows one to realize the infinitesimal chiral transformation on quark fields as $\delta\bar{\psi} = \bar{\psi}\gamma_5, \delta\psi = \hat{\gamma}_5\psi$. Although the $\hat{\gamma}_5$ depends non-locally on the gauge fields, since the G-W is equivalent to $\hat{\gamma}_5^2 = 1$, it does allow an unambiguous definition of chiral projection operators: $\psi_{R/L} = \frac{1}{2}(1 \pm \hat{\gamma}_5)\psi$.

For finite L_s the violation of chiral symmetry is given by the error, $\Delta_{L_s}[H_5]$, in the Ginsparg-Wilson relation:

$$2\gamma_5\Delta_{L_s}[H_5] \equiv \gamma_5 D_{ov}(0) + D_{ov}(0)\gamma_5 - 2D_{ov}(0)\gamma_5 D_{ov}(0) = \frac{1}{2}\gamma_5(1 - \epsilon_L^2[H_5]). \quad (2.5)$$

From Eq. 2.4 this is equivalent to $\Delta_{L_s}[H_5] = (1 + \hat{\gamma}_5)(1 - \hat{\gamma}_5)/4$, which is a natural way to measure the failure to implement exactly the projectors: $\hat{P}_\pm = (1 \pm \hat{\gamma}_5)/2$. This **GW chiral violation operator**, $\Delta_{L_s}[H_5]$, is the unique measure of chiral symmetry violations applicable to any (not necessarily a domain wall) scheme to implement chirality.

To emphasize this point further, consider how global chiral symmetry of the Fermion action,

$$S_{ov}^F = \sum_{xy} \bar{\psi}_x D_{ov}(m)_{xy} \psi_y = \bar{\psi}_x D_{ov}(0)_{xy} \psi_y + m\bar{\psi}_x(1 - D_{ov}(0))\psi_x, \quad (2.6)$$

is modified both by the implicit violation due to an approximate overlap action and by the explicit breaking by the bare quark mass term, m . The mass term ¹ is given in terms of the scalar density,

$$S(x) = \bar{\psi}_x(1 - D_{ov}(x))\psi_x = \bar{\psi}_x \frac{1 + \gamma_5\hat{\gamma}_5}{2}\psi_x, \quad (2.7)$$

paired with the pseudo-scalar,

$$P(x) = \bar{\psi}_x\gamma_5(1 - D_{ov}(x))\psi_x = \bar{\psi}_x \frac{\gamma_5 + \hat{\gamma}_5}{2}\psi_x, \quad (2.8)$$

under the chiral transformation: $\delta S(x) = 2P(x), \delta P(x) = 2S(x)$. At finite L_s following the analysis in Ref. [26], we continue to define the chiral transformation using $\hat{\gamma}_5 = \gamma_5(1 - D_{ov}(0))$. The chiral transformation of the action in Eq. 2.6 now yields two contributions,

$$\delta S_{ov}^F = \bar{\psi}[\gamma_5 D_{ov}(m) + D_{ov}(m)\hat{\gamma}_5]\psi = m\bar{\psi}(\gamma_5 + \hat{\gamma}_5)\psi + 2\bar{\psi}\gamma_5\Delta_L\psi, \quad (2.9)$$

¹We note that the physical range for the mass is $0 \leq m < 1$. Indeed it is tempting therefore to rescale the action by $(1 - m)^{-1}S_{ov}^F = \bar{\psi}_x D_{ov}(0)_{xy} \psi_y + m_q \bar{\psi}_x \psi_x$ defining additive bare quark mass $m_q = m/(1 - m)$ since the limit $m_q \rightarrow \infty$ (or $m = 1$) corresponds to the decoupling of the Domain wall quarks by cancellation with Pauli-Villars operator $D_{PV} = D_{ov}(m = 1)$. However the conventional choice has the advantage of introducing the mass operator as the correct scalar partner $S(x)$ to the pseudo-scalar density $P(x)$.

the first one due to the quark mass and the second one due to the finite L_s approximation, expressed as same GW violation operator, Δ_L^{xy} , defined above in Eq. 2.5. Like the overlap operator itself, this chiral violating operator, Δ_L^{xy} , should also fall off exponentially in units of the lattice spacing so that it may be approximated by an effective Lagrangian,

$$\bar{\psi}\Delta_L\psi \simeq m_{res}\bar{\psi}\psi + c_1\bar{\psi}\gamma_\mu(\partial_\mu - iA_\mu)\psi + ic_2\bar{\psi}\sigma_{\mu\nu}F^{\mu\nu}\psi + c_4\bar{\psi}(\partial_\mu - iA_\mu)^2\psi + \dots, \quad (2.10)$$

expanding in the lattice spacing. The terms in increasing dimension define a residual mass, m_{res} , the 4d wave function renormalization, the 5d operators or the clover term and so on respectively. In Sec. 5.1, we will extend this analysis to examine the local breaking of chiral symmetry in the Ward-Takahashi identities for the axial current. There we show that this same operator, $\bar{\psi}\gamma_5\Delta_L\psi$, is the correction to the divergence for axial current. Its vacuum to pion matrix element is the conventional definition of the residual mass [36, 37, 38].

In spite of the exact mapping between overlap and domain wall Fermions, unfortunately the most common implementations use different kernels. For the overlap it is natural to use the Wilson (or Neuberger/Boriçi) kernel,

$$D^{Borici}(M_5) = a_5 D^{Wilson}(M_5), \quad (2.11)$$

while for the Shamir domain wall implementation [5], the kernel is

$$D^{Shamir}(M_5) = \frac{a_5 D^{Wilson}(M_5)}{2 + a_5 D^{Wilson}(M_5)}, \quad (2.12)$$

where we include in the definition the lattice spacing a_5 in the fifth direction, although it is generally set to $a_5 = 1$ in units of the space-time lattice. Both the Shamir and Neuberger/Boriçi kernels are constructed from the Wilson lattice Dirac operator,

$$D_{xy}^{Wilson}[U_\mu(x), M_5] = (4 + M_5)\delta_{x,y} - \frac{1}{2} \left[(1 - \gamma_\mu)U_\mu(x)\delta_{x+\mu,y} + (1 + \gamma_\mu)U_\mu^\dagger(y)\delta_{x,y+\mu} \right], \quad (2.13)$$

with a negative mass term $M_5 = O(-1)$. Unfortunately the Shamir kernel (2.12) is computationally expensive to use in overlap codes. On the other hand, as first realized by Boriçi [27, 28], the simpler Wilson overlap kernel (2.11) can easily be realized as a domain wall action by adding a specific next to nearest neighbor term in the 5th direction.

Here we found that an equally computationally efficient domain wall action allows one to introduce the generalized kernel,

$$D^{Moebius}(M_5) = \frac{(b_5 + c_5)D^{Wilson}(M_5)}{2 + (b_5 - c_5)D^{Wilson}(M_5)}, \quad (2.14)$$

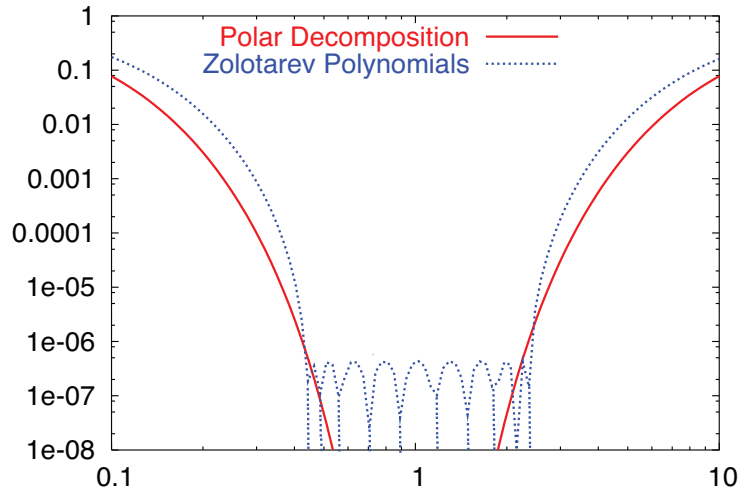


Figure 1: The error, $1 - \epsilon_{L_s}(\lambda)$ for the polar decomposition at $L_s = 16$ is plotted against an eigenvalue of the kernel H_5 for $\lambda \in [0.1, 10]$. In the polar approximation the error is positive semi-definite for $\lambda \geq 0$, anti-symmetric for $\lambda \rightarrow -\lambda$ and symmetric under $\lambda \rightarrow 1/\lambda$. This is compared with $|1 - \epsilon_{L_s}(\lambda)|$ for the Zolotarev polynomial at $L_s = 10$ whose error fluctuates in sign.

referred to as Möbius Fermions because the 3 parameters M_5, b_5, c_5 are equivalent to a real Möbius transformation, $D^{Wilson}(-1) \rightarrow [a + bD^{Wilson}(-1)]/[c + dD^{Wilson}(-1)]$, of the Wilson operator – the most general conformal map preserving the real axis. It encompasses both the Shamir and Boriçi form as special cases. Obviously the standard polar decomposition for the Shamir kernel is recovered with $b_5 = a_5$ and $c_5 = 0$ while the Boriçi truncated overlap action is implemented for $b_5 = c_5 = a_5$. In addition to the Shamir parameter, $a_5 = b_5 - c_5$, there is a new scale factor, $\alpha = (b_5 + c_5)/a_5$, which turns out to have a major impact on reducing chiral symmetry violation at finite L_s . Just rescaling the Shamir kernel we have

$$D^{Moebius}(M_5) = \alpha \frac{a_5 D^{Wilson}(M_5)}{2 + a_5 D^{Wilson}(M_5)} \equiv \alpha D^{Shamir}(M_5). \quad (2.15)$$

We will also extend our analysis to s-dependent coefficients, $a_5(s) = b_5(s) - c_5(s)$, $\alpha(s)a_5(s) = b_5(s) + c_5(s)$, so that this presentation includes the Zolotarev approximation (for example) as described in Ref [39, 40]. See Fig. 1 for an illustration of the error in the sign function for the polar versus the Zolotarev approximation.

The scaling parameter plays a particularly important role in Möbius Fermions. Since the sign function is scale invariant, if we simply rescale the Shamir action, $\epsilon_{L_s}[H_5] = \epsilon_{L_s/\alpha}[\alpha H_5]$, the Möbius action is identical to the Shamir action in the $L_s \rightarrow \infty$ limit. Thus it is proper to

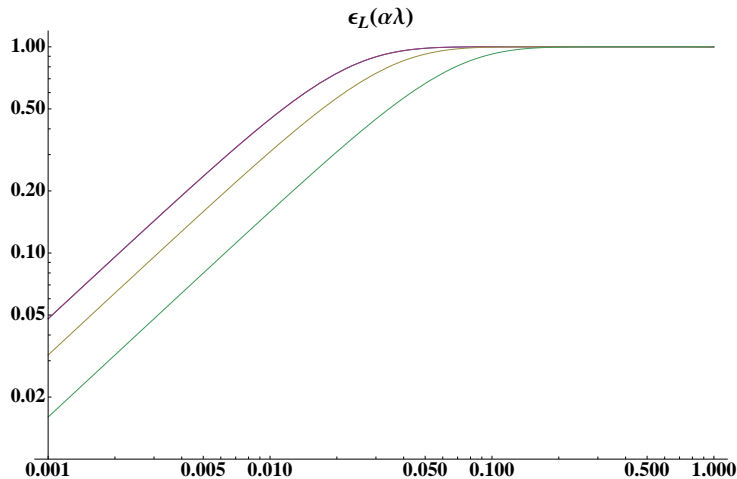


Figure 2: The top curve represents the sign function $\epsilon_{L_s}(\alpha\lambda)$ plotted against λ for Shamir ($\alpha = 1$) at $L_s = 48$ compared with scaled Möbius ($\alpha = 4$) at $L_s = 12$, which are indistinguishable on a loglog plot. This contrast with the middle and lower curves for Shamir at $L_s = 32$ and $L_s = 16$ respectively which do degrade the chiral approximation substantial.

regard this as a new algorithm with improved chirality at finite L_s . A heuristic explanation for this is easily understood. Consider how the polar approximation in Eq. 2.2,

$$\epsilon_{L_s}(H_5) = \sum_{\lambda} |\lambda| \epsilon_{L_s}(\lambda) \langle \lambda |, \quad (2.16)$$

in the spectral representation approaches the sign function $\epsilon(H_5)$. The polar approximation, illustrated in Fig. 1, is exact at $\lambda = \pm 1$ and has an error $\Delta_{L_s}(\lambda) = (1 - \epsilon_{L_s}^2(\lambda))/4$ that satisfies the inversion symmetry $\Delta_{L_s}(\lambda) = \Delta_{L_s}(1/\lambda)$. It converges exponentially for increasing L_s in a window $O(1/L_s) < |\lambda| < O(L_s)$. However since the spectrum of H_5 is bounded $|\lambda| \leq \lambda_{max}$ the upper end of the window is wasted whenever $L_s > O(\lambda_{max})$. Consequently by using the Möbius scaling parameter α , the log spectrum can be shifted and for $\alpha\lambda_{max} < O(L_s)$ we take advantage of the entire window in the polar approximation, greatly improving the approximation for the small eigenvalues with essentially no damage to the approximation at the high end of the eigenvalue spectrum. For example with the Shamir kernel with $a_5 = 1$, $\lambda_{max} \simeq (8 - M_5)/(10 - M_5) \simeq 3/4$ so we can rescaling the Shamir kernel by $\alpha = O(L_s)$ allowing the window to cover better the low eigenvalues that are mostly responsible for the observed explicit chiral symmetry breaking.

In addition note that for low eigenvalues and typical values of α (such as those used in our numerical tests), the sign function obeys the scaling rule, $\epsilon_{L_s}(\lambda) \simeq \epsilon_{L_s/\alpha}(\alpha\lambda)$. Indeed as

illustrated in Fig. 2, this scaling rule holds quite well for a substantial part of the low end of the spectral range of the Hermitian kernel H_5 so the Domain Wall operator is essentially unchanged under this “approximate equivalence relation”:

$$\textbf{Scaling Rule:} \quad \text{Shamir at } L_s \simeq \text{Möbius at } L_s/\alpha . \quad (2.17)$$

Since each eigenvector of the operator and therefore the operator itself is preserved, the Möbius rescaling can be understood as an improved algorithm for essentially the same lattice Dirac action. For codes requiring an aggressive chiral approximation, the advantage of the Möbius algorithm will be dramatic. For example, recently the Shamir domain simulation have required $L_s = 48$ for $\mathcal{N} = 1$ SUSY [32] and $L_s = 32$ for thermodynamics [31] or even larger L_s to get sufficiently small m_{res} . However as demonstrated in Fig. 2 the rescaling from Shamir at $L_s = 48$ to Möbius at $L_s = 12$ and $\alpha = 4$ has no visible effect on a loglog plot. The difference is $|\epsilon_{48}[\lambda] - \epsilon_{12}[4\lambda]| < 10^{-3}$ for all the vectors of H_5 . Consequently any simulation using $L_s = 32$ or larger should benefit very substantially by a factor of 2-4 using Möbius in the range of $L_s = 12$ to 16 with equally small values of m_{res} .

2.1 Domain Wall Action for Möbius Fermions

We now proceed to construct the domain wall action that gives rise to the Möbius kernel. It is useful to introduce two generalized kernels:

$$D_+^{(s)} = b_5(s)D^{Wilson}(M_5) + 1 \quad \text{and} \quad D_-^{(s)} = c_5(s)D^{Wilson}(M_5) - 1, \quad (2.18)$$

with $s = 1, 2, \dots, L_s$. We keep an arbitrary s -dependence to allow for generalization of our formulation to other five dimensional approximations to the overlap such as the Zolotarev polynomial approximation. Also the s -dependence of $D_+^{(s)}$ and $D_-^{(s)}$ allows for generalizations to formulations that require a gauge field dependence of the fifth dimension such as the domain wall filters suggested in Ref. [41]. Now our generalized domain wall Fermion action ² is

$$\begin{aligned} \bar{\Psi}D^{DW}(m)\Psi &= \sum_{s=1}^{L_s} \bar{\Psi}_s D_+^{(s)} \Psi_s + \sum_{s=2}^{L_s} \bar{\Psi}_s D_-^{(s)} P_+ \Psi_{s-1} + \sum_{s=1}^{L_s-1} \bar{\Psi}_s D_-^{(s)} P_- \Psi_{s+1} \\ &- m \bar{\Psi}_1 D_-^{(1)} P_+ \Psi_{L_s} - m \bar{\Psi}_{L_s} D_-^{(L_s)} P_- \Psi_1, \end{aligned} \quad (2.19)$$

where we follow the conventions of Edwards and Heller [25], placing the left chiral modes, $q^L = P_- \Psi_1$ on the $s = 1$ wall and the right chiral modes, $q^R = P_+ \Psi_{L_s}$ on the $s = L_s$ wall as

²Through out we adopt the convention of upper case for 5d domain wall fields (e.g. $\Psi_{x,s}$) and lower case for 4d overlap fields (e.g. ψ_x) and 4d domain wall fields on the boundary (e.g. $q = [\mathcal{P}^\dagger \Psi]_1$).

depicted in Fig 3. $P_{\pm} = \frac{1}{2}(1 \pm \gamma_5)$ are the chiral projectors. Written as an $L_s \times L_s$ tridiagonal matrix the Möbius operator is

$$D^{DW}(m) = \begin{bmatrix} D_+^{(1)} & D_-^{(1)} P_- & 0 & \cdots & -m D_-^{(1)} P_+ \\ D_-^{(2)} P_+ & D_+^{(2)} & D_-^{(2)} P_- & \cdots & 0 \\ 0 & D_-^{(3)} P_+ & D_+^{(3)} & \cdots & 0 \\ \cdots & \cdots & \cdots & \cdots & \cdots \\ -m D_-^{(L_s)} P_- & 0 & 0 & \cdots & D_+^{(L_s)} \end{bmatrix}. \quad (2.20)$$

For the polar decomposition, it is sufficient to choose constant coefficients $b_5(s) = b_5$, $c_5(s) = c_5$ for all s with the kernel taking the form,

$$D^{Moebius}(M_5) = \frac{(b_5 + c_5) D^{Wilson}(M_5)}{2 + (b_5 - c_5) D^{Wilson}(M_5)} = \frac{D_+ + D_-}{D_+ - D_-}. \quad (2.21)$$

It is worth noting that there maybe a computational advantage to placing the chiral projectors, P_{\pm} , to the left of $D_-^{(s)}$. Converting to this form is a trivial similarity transformation, $D^{DW}(m) \rightarrow \hat{D}^{DW}(m) = D_-^{-1} D^{DW}(m) D_-$ where we introduce the matrix,

$$D_- = \text{Diag} \left[D_-^{(1)} \quad D_-^{(2)} \quad D_-^{(3)} \quad \cdots \quad D_-^{(L_s)} \right],$$

diagonal in the 5th axis. Assuming reflection symmetry $D_-^{(s)} = \mathcal{R}_{ss'} D_-^{(s')} = D^{(L_s+1-s)}$ the generalization of γ_5 -Hermiticity is

$$\Gamma_5 D^{DW}(m) = D^{\dagger DW}(m) \Gamma_5. \quad (2.22)$$

Here $\Gamma_5 = \gamma_5 \mathcal{R} D_-^{-1}$ is defined to include inverting the 5-th axis,

$$\mathcal{R}_{ss'} = \delta_{L_s+1-s,s'}, \quad (2.23)$$

and rescaling by D_-^{-1} . The fact that $H^{DW} = \gamma_5 \mathcal{R} D_-^{-1} D^{DW}(m)$ is a Hermitian operator guarantees that the effective 4d overlap operator is “ γ_5 Hermitian”³.

2.2 Domain Wall to Overlap Reduction

The equivalence between domain wall and overlap Fermions (which has been established in the literature as discussed in the introduction) is constructed by dimensional reduction from 5 to 4

³In terms of the transfer operator on the $(s+1, s)$ link introduced later this condition is $T_s = T_{L_s+1-s}$. In the case of the Zolotarev approximation, one uses the condition that s-dependent transfer matrix commutator vanishes ($[T_s, T_{s'}] = 0$) to show γ_5 Hermiticity of the 4d effective operator.

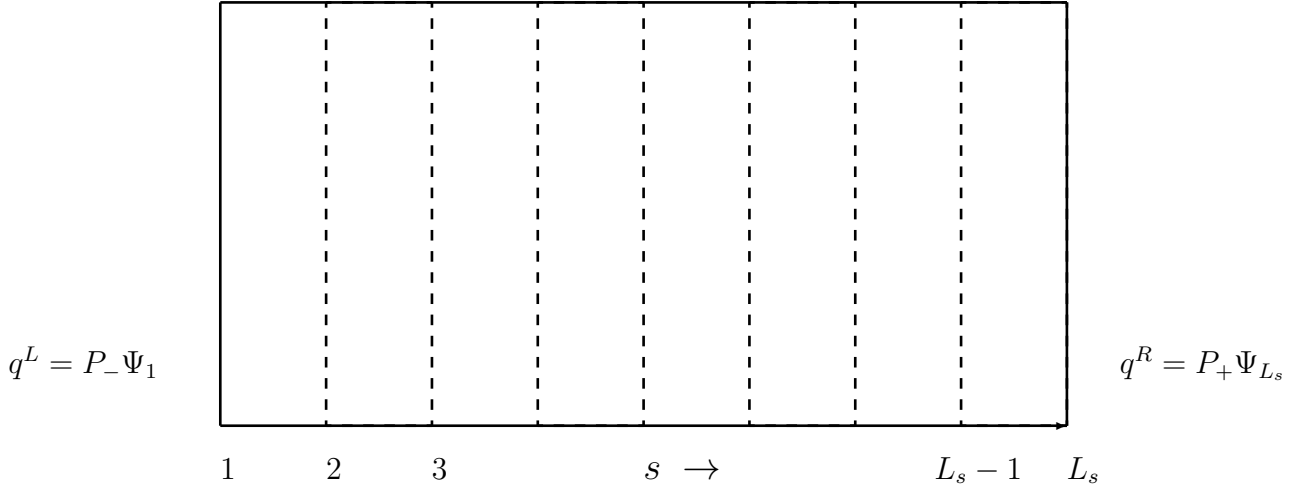


Figure 3: Domain wall convention with the physics Right/Left chiral mode at $s = 1$ and $s = L_s$ respectively for an approximation of the fifth dimension by width $a_5 L_s$. The Pauli-Villars operator has anti-periodic boundary condition and the Dirac operator Dirichlet boundary condition at zero quark mass.

dimensions ⁴ Since the Fermion action is quadratic, there is an explicit map to the 4d overlap operator from the 5d domain wall action. To accomplish this is a straight forward application of **LDU decomposition** for both the Dirac, $(D^{DW}(m)\mathcal{P})$ and Pauli-Villars $(D^{DW}(1)\mathcal{P})$ matrices, as demonstrated in Appendix A. This procedure makes use of a permutation matrix,

$$\mathcal{P} = \begin{bmatrix} P_- & P_+ & \cdots & 0 \\ 0 & P_- & P_+ \cdots & 0 \\ \vdots & \vdots & \ddots & \vdots \\ 0 & 0 & \cdots & P_+ \\ P_+ & 0 & \cdots & P_- \end{bmatrix}, \quad (2.24)$$

This matrix, $\mathcal{P}_{ss'} = \delta_{ss'} P_- + \delta_{s',(s+1) \bmod L_s} P_+$, is a unitary permutation, $\mathcal{P}^{-1} = \mathcal{P}^\dagger = \mathcal{R}\mathcal{P}\mathcal{R}$, which rotates the positive chiral mode at $s = L_s$ to the same position as the left chiral mode at $s = 1$, so that the new 4d Dirac field is reassembled at $s = 1$:

$$q_x = P_- \Psi_{x,1} + P_+ \Psi_{x,L_s} = [\mathcal{P}^\dagger \Psi]_{x,1}. \quad (2.25)$$

The main result of the LDU decomposition in Appendix A is that we are led to consider

⁴The details of the formulation discussed here first appeared in [17].

the domain wall Dirac operator preconditioned by the Pauli-Villars (corresponding to infinite quark mass) operator,

$$K^{DW}(m) = \mathcal{P}^\dagger \frac{1}{D^{DW}(1)} D^{DW}(m) \mathcal{P} . \quad (2.26)$$

This matrix has a remarkably simple form given by

$$K^{DW}(m) = \mathcal{P}^\dagger \frac{1}{D^{DW}(1)} D^{DW}(m) \mathcal{P} = \begin{bmatrix} D_{ov}(m) & 0 & 0 & \cdots & \cdots & \cdots & 0 \\ -(1-m)\Delta_2^R & 1 & 0 & 0 & \cdots & \cdots & 0 \\ -(1-m)\Delta_3^R & 0 & 1 & 0 & \cdots & \cdots & 0 \\ -(1-m)\Delta_4^R & 0 & 0 & 1 & \cdots & \cdots & 0 \\ \vdots & \vdots & \ddots & \ddots & \ddots & \ddots & \vdots \\ -(1-m)\Delta_{L_s}^R & 0 & \cdots & \cdots & \cdots & \cdots & 0 & 1 \end{bmatrix} . \quad (2.27)$$

Its inverse, or propagator matrix, has the form

$$A^{DW}(m) = \mathcal{P}^\dagger \frac{1}{D^{DW}(m)} D^{DW}(1) \mathcal{P} = \begin{bmatrix} D_{ov}^{-1}(m) & 0 & 0 & \cdots & \cdots & \cdots & 0 \\ (1-m)\Delta_2^R D_{ov}^{-1}(m) & 1 & 0 & 0 & \cdots & \cdots & 0 \\ (1-m)\Delta_3^R D_{ov}^{-1}(m) & 0 & 1 & 0 & \cdots & \cdots & 0 \\ (1-m)\Delta_4^R D_{ov}^{-1}(m) & 0 & 0 & 1 & \cdots & \cdots & 0 \\ \vdots & \vdots & \ddots & \ddots & \ddots & \ddots & \vdots \\ (1-m)\Delta_{L_s}^R D_{ov}^{-1}(m) & 0 & \cdots & \cdots & \cdots & \cdots & 0 & 1 \end{bmatrix} . \quad (2.28)$$

The results for the K^{DW} matrix in Eq. 2.27 and its inverse in Eq. 2.28 play a fundamental role in understanding the dynamics of the domain wall Fermion construction. They state the remarkable fact, that once the domain wall Fermion operator, $D^{DW}(m)$, is “preconditioned” by the Pauli-Villars operator, $D^{DW}(1)$, the propagation into the fifth dimension from the chiral domain wall is “instantaneous”. All the essential properties are independent of the particular structure of the domain wall operator. The “instantaneous” property is easily demonstrated by rewriting the propagator as the sum of two terms,

$$\mathcal{P}^\dagger \frac{1}{D^{DW}(m)} D^{DW}(1) \mathcal{P} = 1 + \mathcal{P}^\dagger \frac{1}{D^{DW}(m)} (D^{DW}(1) - D^{DW}(m)) \mathcal{P} . \quad (2.29)$$

The first term contributes exclusively to the non-zero value on the diagonal and the second to the first column,

$$[(D^{DW}(1) - D^{DW}(m)) \mathcal{P}]_{s',s} = -(1-m) D_-^{(s')} \mathcal{P}_{s',1} \delta_{s,1} , \quad (2.30)$$

because the mass parameter in the domain wall operator is restricted to the link connecting the left and right walls. The zeros in the above equation represent the cancellation between bulk

modes of the Dirac and Pauli-Villars terms. In the continuum the cancellation occurs [42] for all off-diagonal terms but otherwise is very similar.

The non-zero elements depend only on the transfer matrix along the 5th dimension,

$$T_s = \frac{1 - H_s}{1 + H_s} \quad \text{with} \quad H_s = \gamma_5 \frac{(b_5(s) + c_5(s))D^{Wilson}(M_5)}{2 + (b_5(s) - c_5(s))D^{Wilson}(M_5)}. \quad (2.31)$$

The effective overlap operator is then given by

$$D^{ov}(m) = \frac{1 + m}{2} + \frac{1 - m}{2} \gamma_5 \frac{\mathbb{T}^{L_s} - 1}{\mathbb{T}^{L_s} + 1}, \quad (2.32)$$

where $\mathbb{T}^{-L_s} \equiv T_1^{-1} T_2^{-1} \dots T_{L_s}^{-1}$. The rest of the first column are built out of partial ordered products

$$\Delta_s^L = \frac{T_1^{-1} T_2^{-1} \dots T_s^{-1}}{1 + \mathbb{T}^{-L_s}} \quad , \quad \Delta_{s+1}^R = \frac{T_{s+1}^{-1} T_{s+2}^{-1} \dots T_{L_s}^{-1}}{1 + \mathbb{T}^{-L_s}}. \quad (2.33)$$

We also note that the GW violation operator, Δ_{L_s} , in Eq. 2.5 has a similar expression joining the left and right wall,

$$\Delta_{L_s} = \Delta_s^L \Delta_{s+1}^R = \left[\frac{1}{\mathbb{T}^{-L_s/2} + \mathbb{T}^{L_s/2}} \right]^2 = \frac{1}{4} \left[1 - \epsilon_{L_s}^2(H_5) \right]. \quad (2.34)$$

Clearly convergence to the exact chiral limit, $\Delta_{L_s \rightarrow \infty} = 0$, depends on the spectrum of the transfer operator as is evident in the original construction of the overlap operator by Neuberger et al [7, 8, 10].

2.3 Overlap to bulk Domain Wall reconstruction

We can essentially reverse the 5d to 4d dimensional reduction at a small cost using the more easily inverted Pauli-Villars operator. This is useful in a variety of instances, the most obvious being the reconstruction of the full domain wall solution, when you have only saved the solution to the effective overlap propagator. Another recent example is the use of a Möbius operator at small L_s as a preconditioner for larger L_s standard Shamir operator, as in the recent Möbius Accelerated Domain Wall Fermion (MADWF) algorithm [20].

Let's begin by assuming we have the solution to the effective overlap equation,

$$D_{ov}(m)\psi = b, \quad (2.35)$$

and proceed to find the domain wall propagator assuming that its source is given by $B_s = b \delta_{s,1}$ on the boundary. The goal is to reconstruct the 5d bulk propagator. In the first step using Eq. 2.27 and defining, $\tilde{\psi}_s = \psi \delta_{s,1}$, we reconstruct the vector in the interior,

$$\Omega = \mathcal{P}^\dagger \frac{1}{D^{DW}(1)} D^{DW}(m) \mathcal{P} \tilde{\psi} = \begin{bmatrix} D_{ov} \psi \\ -(1-m) \Delta_2^R \psi \\ -(1-m) \Delta_3^R \psi \\ \vdots \\ -(1-m) \Delta_{L_s}^R \psi \end{bmatrix}. \quad (2.36)$$

with the cost of having to invert the Pauli-Villars matrix. Using Eq. 2.28 we see that the 5d solution Ψ is given by

$$\Psi = \mathcal{P}^\dagger \frac{1}{D^{DW}(m)} D^{DW}(1) \mathcal{P} B = \begin{bmatrix} \psi \\ (1-m) \Delta_2^R \psi \\ (1-m) \Delta_3^R \psi \\ \vdots \\ (1-m) \Delta_{L_s}^R \psi \end{bmatrix}, \quad (2.37)$$

where $B_s = b \delta_{s,1}$ is a 5d vector with support on the boundary only.

Comparing the two results we have

$$\Psi_s^{dwf} = \text{diag}(D_{ov}^{-1}, -1, \dots, -1) \Omega = \begin{cases} \psi & s = 1 \\ -\Omega_s & s \neq 1 \end{cases}. \quad (2.38)$$

This final step only requires flipping the sign, $\Psi_s = -\Omega_s$ for $s = 2, \dots, L_s$. The cost of this construction is the cost of solving a 5d linear system for the Pauli-Villars matrix which converges in $O(50)$ conjugate gradient iterations for typical applications.

Using this formulation we can construct the conserved axial-vector and vector current matrix elements using only the stored overlap propagators. Furthermore, we can use this formalism to define prolongation and restriction operations to coarsen the fifth dimension in the spirit of a multigrid solver. However it should be realized that a true domain wall multigrid algorithm [24] requires blocking in the 4d to overcome the critical slowing down in the chiral limit.

2.4 4d Hybrid Monte Carlo

Another related consequence of the fundamental identity in Eq. 2.28 is the ability to reformulate Hybrid Monte Carlo evolution for domain wall Fermions restricting the pseudo-fermions to the

wall. For example consider the standard approach to HMC in using domain wall Fermions in dynamical Fermion calculations [43, 44]

$$\det[D_{ov}^\dagger D_{ov}] = \int d\phi_1 \cdots d\phi_{L_s} e^{-\phi^\dagger \mathcal{P}^\dagger D^{\dagger DW}(1) \frac{1}{D^{DW}(m)^\dagger} \frac{1}{D^{DW}(m)} D^{DW}(1) \mathcal{P} \phi}. \quad (2.39)$$

for 2 flavor example that introduces pseudo-fermions ϕ_s in the bulk. If we look at the action $S(\phi^\dagger, \phi)$,

$$\begin{aligned} S(\phi^\dagger, \phi) &= \phi_1^\dagger \frac{1}{D_{ov}^\dagger} \frac{1}{D_{ov}} \phi_1 \\ &+ \sum_{s=2}^{L_s} [\phi_s + (1-m)\Delta_s^R D_{ov}^{-1} \phi_1]^\dagger [\phi_s + (1-m)\Delta_s^R D_{ov}^{-1} \phi_1], \end{aligned} \quad (2.40)$$

we see that only the first term contributes to the path integral. The remaining terms integrate to unity trivially but they do add unwanted noise to the stochastic estimator.

From the reconstruction procedure described above the bulk degrees of freedom should be redundant. Indeed this is true if we use the identity

$$(D_{ov}^\dagger(m) D_{ov}(m))^{-1} = [A^{DW} A^{DW\dagger}]_{11} = [\mathcal{P}^\dagger \frac{1}{D_{DW}(m)} D_{DW}(1) D_{DW}^\dagger(1) \frac{1}{D_{DW}^\dagger(m)} \mathcal{P}]_{11} \quad (2.41)$$

that follows from Eq. 2.28 to rewrite the determinant in terms of pseudoFermions restricted to $s = 1$.

$$\det[D_{ov}^\dagger D_{ov}] = \int d\phi_1 e^{-\phi_1^\dagger \mathcal{P}^\dagger \frac{1}{D_{DW}(m)} D_{DW}(1) D_{DW}^\dagger(1) \frac{1}{D_{DW}^\dagger(m)} \mathcal{P} \phi_1}. \quad (2.42)$$

The benefit of removing the redundant random pseudo-fermions from the bulk may be significant. Unfortunately, we should also note that the force term now requires two inversions instead of one as seen from the expression,

$$\begin{aligned} F_\mu &= \delta_{\omega_\mu} \left[\phi^\dagger \mathcal{P}^\dagger D_{DW}^{-1}(m) D_{DW}(1) D_{DW}^\dagger(1) D_{DW}^{-1}(m) \mathcal{P} \phi \right] \\ &= \chi^\dagger \delta_{\omega_\mu} [D_{DW}(m)] \psi + \psi^\dagger \delta_{\omega_\mu} [D_{DW}^\dagger(m)] \chi + \chi^\dagger \delta_{\omega_\mu} [D_{DW}(1) D_{DW}^\dagger(1)] \chi, \end{aligned} \quad (2.43)$$

in terms of auxiliary χ and ψ fields defined as,

$$\begin{aligned} \chi &= D_{DW}^{-1}(m) \mathcal{P} \phi, \\ \psi &= D_{DW}^{-1}(m) D_{DW}(1) D_{DW}^\dagger(1) \chi. \end{aligned} \quad (2.44)$$

The extra cost of the second inversion might be acceptable due to better scaling for large L_s or be compensated by better inversion algorithms for the first order system. Exploring these possibilities is beyond the scope of this paper.

Finally, using the formalism described above we can formulate a preconditioned HMC using a small L_s domain wall operator as a preconditioner. Then using a multiple time scale integrator, one can run most of the calculation using the small L_s operator. The correction step which will require the inversion of the large L_s matrix will only be needed a few times during a trajectory. The precise implementation as well as the possible interplay with the Hasenbush preconditioner requires detailed experimentation for finding the optimal HMC algorithm for DWF dynamical calculations. Here we simply suggest one more trick to be used together with the rest of today's HMC methodology.

3 Red Black Preconditioning

In order to place the performance of Möbius on an equal footing with Shamir Fermions, it is essential to implement red-black preconditioning. For the standard Shamir implementations, this step alone accounts for nearly a factor of 3 speed up. However the standard 5d even-odd preconditioning is not efficient for the Möbius generalization because the new Wilson operator D_- connects 5d even and odd sites ($x \pm \mu$ and $s \pm 1$). This preconditioning would require a Wilson operator inverse as a new inner loop. This problem also occurs for the Boriçi domain wall action and continued fraction approach to the Overlap operator and in general whenever the hopping terms for the effective “fifth” dimension is coupled to the spatial lattice.

To avoid this problem we define a new red-black partitioning that uses a 4d red-black lattice without alternating color as you run along the 5-th axis. The result is a red-red and black-black matrix that is tridiagonal with constant coefficients. The specific construction is as follows. Red-black is chosen as checkerboard on the space-time lattice as $x_1 + x_2 + x_3 + x_4 = \text{even/odd}$ for all $s \in [0, L_s]$. The hopping matrix in 5d are D_{br}^{DW} and D_{rb}^{DW} so

$$D^{Wilson}(M) = \begin{bmatrix} I_{rr} & D_{rb}^{DW} \\ D_{br}^{DW} & I_{bb} \end{bmatrix}, \quad (3.1)$$

with Schur decomposition,

$$D_{DW}(M) = \begin{bmatrix} 1 & 0 \\ D_{br}^{DW} I_{rr}^{-1} & 1 \end{bmatrix} \begin{bmatrix} I_{rr} & 0 \\ 0 & I_{bb} - D_{br}^{DW} I_{rr}^{-1} D_{rb}^{DW} \end{bmatrix} \begin{bmatrix} 1 & I_{rr}^{-1} D_{rb}^{DW} \\ 0 & 1 \end{bmatrix}, \quad (3.2)$$

leads to the red-black Schur complement (or preconditioned matrix):

$$D_{pre}^{DW} = 1 - I_{bb}^{-1} D_{br}^{DW} I_{rr}^{-1} D_{rb}^{DW}. \quad (3.3)$$

With $M_+ = b_5(4 + M_5) + 1$ and $M_- = c_5(4 + M_5) - 1$, the diagonal blocks in 5d are

$$I_{rr} = I_{bb} = \begin{bmatrix} M_+ & M_-P_- & 0 & \cdots & -mP_+ \\ M_-P_+ & M_+ & M_-P_- & \cdots & 0 \\ 0 & M_-P_+ & M_+ & \cdots & 0 \\ \vdots & \vdots & \vdots & \ddots & \vdots \\ -mM_-P_- & 0 & 0 & \cdots & M_+ \end{bmatrix}. \quad (3.4)$$

These can easily be inverted with the observation that $I_{rr} = A_{rr}P_- + A_{rr}^T P_+$ where

$$A_{rr} = M_+ \begin{bmatrix} 1 & M_-/M_+ & 0 & \cdots & 0 \\ 0 & 1 & M_-/M_+ & \cdots & 0 \\ 0 & 0 & 1 & \cdots & 0 \\ \vdots & \vdots & \vdots & \ddots & \vdots \\ -mM_-/M_+ & 0 & 0 & \cdots & 1 \end{bmatrix}. \quad (3.5)$$

To find the inverse $I_{rr}^{-1} = A_{rr}^{-1}P_- + A_{rr}^{T-1}P_+$, we solve $A_{rr}\Psi_L = b_L$ and $A_{rr}^\dagger\Psi_R = b_R$ independently for each chiral sector. This is performed by Gauss elimination of $O(L_s)$ steps of multiply-add and one division for half the lattice points per site in the space-time volume. There is no communication if the s-axis is inside the processing element. The computation cost is negligible in comparison with single Dirac applications.

The closed form solution of $A_{rr}\Psi = b$ with $\alpha = M_-/M_+$ and $M = mM_-/M_+$ is first found for $s = L_s$ by forward eliminations,

$$\Psi_{L_s} = \frac{1}{M_+ (1 - M (-\alpha)^{L_s-1})} [b_L + M \sum_{s=1}^{L_s-1} (-\alpha)^{s-1} b_s], \quad (3.6)$$

and the rest for $s = 1, \dots, L_s - 1$ by back substitution,

$$\Psi_s = -\alpha\Psi_{s+1} + \frac{b_s}{M_+}. \quad (3.7)$$

The same procedure interchanging rows and columns solves, $A_{rr}^T\Psi = b$. However we emphasize that in the code it is best to do Gaussian elimination on the fly rather than store the matrix inverse.

Our new (4d) red-black preconditioning for Shamir Fermions is performing as well as the original 5d red-black preconditioning in terms of iteration count. For Möbius Fermions the speed up due to our variant of red-black preconditioning is about a factor 2.5 for our present lattice set. In fact the new version which treats all 5-th axis sites uniformly at fixed

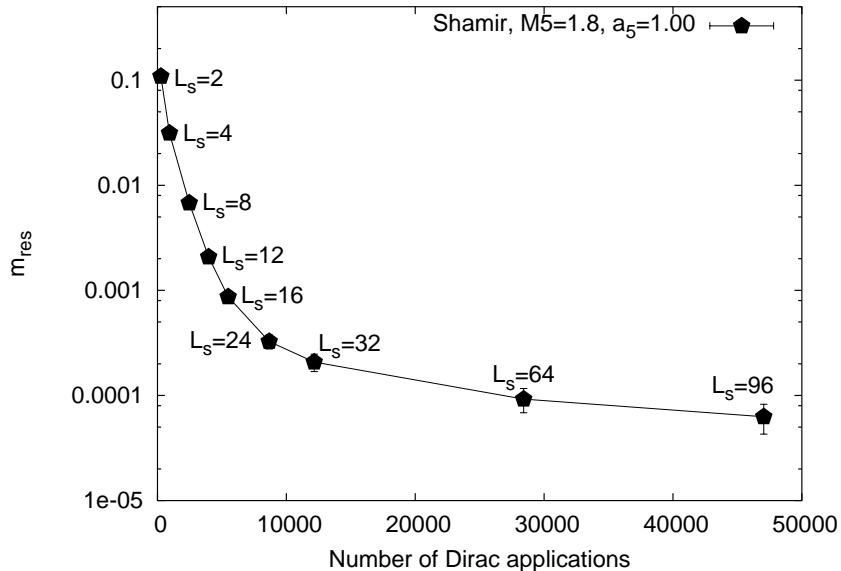


Figure 4: L_s dependence of the residual mass versus the number of Wilson Dirac applications required to invert the standard Shamir operator with $M_5 = 1.8$ and $a_5 = 1$ at $m = 0.06$.

x is advantageous in fast assembly level code for vector pipelines such as those found in Intel processors. Combining this with better data layout using Morton data layout, the Shamir version of the Möbius Domain Wall Fermion (MDWF) code of Pochinsky [21] has achieved a factor 2 improvement relative to earlier implementations.

4 Numerical Results

We have made a series of tests of the effectiveness of the Möbius operator relative to the standard Shamir formulation. For the Shamir formulation (2.12) where a_5 is fixed to 1, one tunes the Wilson mass M_5 and the extent of the fifth dimension L_s in order to achieve the desired degree of approximation to the exactly chiral Dirac operator. While the violation of chirality as measured by m_{res} appears to decrease exponentially at first for increasing L_s , it quickly slows down asymptotically to an $O(1/L_s)$ power fall off [45, 46, 47] as illustrated in Fig. 4.

In the Möbius kernel (2.14) in addition to M_5 and L_s , there are two more parameters, the lattice spacing in 5th dimension, $a_5 = b_5 - c_5$, and the scaling parameter, $\alpha = b_5 + c_5$. The parameter a_5 represents a modification of H_5 and allows us to interpolate between the Boriçi

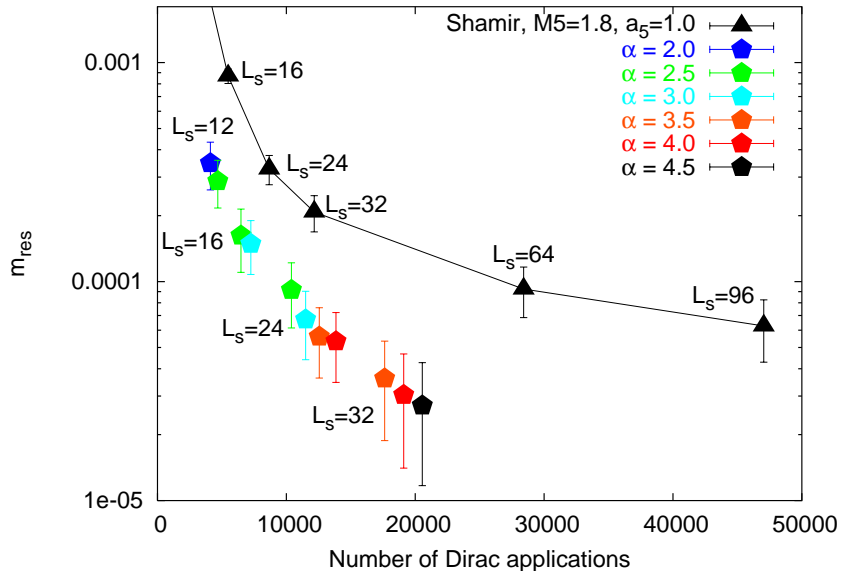


Figure 5: The residual mass for the Möbius algorithm as a function of L_s and α at fixed $M_5 = 1.5$, $a_5 = 1$ and $m = 0.06$ in comparison with the standard Shamir algorithm of Fig. 4.

kernel and the Shamir kernel. However the essential parameter in our scheme is the scaling parameter, α , which allows us to optimize the window (see Fig. 1) for the sign function (2.2) at fixed L_s . Before describing the details of our numerical investigation, we present in Fig. 5 a summary of the result of minimizing the chiral violation as measured by m_{res} at fixed L_s . This clearly shows the importance of choosing an optimal value of $\alpha(L_s)$ as a function of L_s . It is remarkable that the residual mass now appears to continue to fall exponentially with L_s , if we allow this re-tuning of α as L_s increases. However in Sec. 6.5 we argue that a tuned Möbius algorithm eventually falls asymptotically as $O(1/L_s^2)$, in contrast to the standard Shamir action, which shows a much earlier cross over from exponential to $O(1/L_s)$ power behavior at large L_s .

For very small m_{res} the Möbius formulation has the potential for orders of magnitude reduction of the explicit chiral symmetry breaking at fixed computational cost. For example in our test case, residual masses 6×10^{-4} and 3×10^{-5} were achieved at $L_s = 24$ and $L_s = 32$ respectively. Achieving the same residual masses with the Shamir formulation would apparently require a prohibitively large domain wall separations of order $L_s = 10^2$ and $L_s = 10^3$ respectively. This observation is consistent with the estimate of an $O(1/L_s)$ vs $O(1/L_s^2)$ asymptotic fall off of m_{res} for the standard Shamir algorithm vs the improved Möbius algorithm.

4.1 Testing procedure

We have run a large number of tests but for simplicity we present here an optimization study based only on a small sample of 20 quenched $\beta = 6.0$ Wilson gauge action configurations available from the Gauge Connection archive. In spite of this small test sample, we believe the lessons we have learned here are general based on our understanding of how the Möbius formulation works.

Before we proceed in presenting the details of our testing procedure, we note that one Möbius operator application does not need more Wilson Dirac operator applications than the standard Shamir operation at the same L_s . At first glance one might think that this is not the case due to the occurrence of the additional off diagonal terms (2.20) to $s \pm 1$ with the Wilson Dirac operator. However by first taking a vector gather of the neighboring Dirac spinors at $s + 1, s, s - 1$ no additional Dirac applications are required. The additional vector operation on the spinor is insignificant and can be ignored in the total cost estimates. In addition, in order to achieve convergence of the conjugate gradient solver for the Möbius operator similar that achieved for the Shamir operator, the new 4d Red/Black preconditioning described in Sec. 3 had to be invented. This preconditioning also adds an insignificant amount of extra computation. In all the graphs, the label *number of Dirac applications* represents the product of L_s times the number of iterations per source to fixed precision.

In comparing the residual chiral symmetry breaking and the cost of the quark propagator calculation between different values of the parameters, we have at our disposal, we are faced with the fact that the quark mass renormalization factor changes as one changes the kernel operator H_5 . Hence estimating the cost of the calculation at constant physics, and the physical residual chiral symmetry breaking is tricky. In order to resolve this issue, we adopted the following scheme in tuning our bare quark masses. First, as a point of reference for all our tests we adopted the Shamir operator with $M_5 = 1.8$ (with $a_5 = 1.0$ and $\alpha = 1.0$ in Möbius parameterization). The RBC collaboration found in [36, 38] that this M_5 is optimal for the $\beta = 6.0$ Wilson gauge action quenched ensemble. This was followed by a variation of the quark mass on the Möbius side, until the pion mass agreed with that obtained using the standard Shamir action. The renormalization factors, Z_m , is the ratio of the Shamir bare quark mass to the Möbius bare quark mass needed to obtain equal residual masses.

From the data in Table 1, we can deduce that the quark mass renormalization factor Z_m is mostly sensitive to the parameter $a_5 = b_5 - c_5$. All other parameters induce very small variations on this renormalization factor. For that reason, in comparing residual masses between different sets of parameters, only the non-trivial dependence of Z_m on a_5 has to be taken into

account. In all our tests the Shamir quark mass we used is $m = 0.06$ which gave us a pion mass of roughly, $m_\pi = 0.44$ in lattice units.

m	a_5	m	M_5	m	L_s
0.130	2.00	0.093	1.3	0.091	12
0.109	1.75	0.092	1.4	0.091	16
0.091	1.50	0.091	1.5	0.091	24
0.075	1.25	0.090	1.6	0.091	32
0.065	1.00				
0.055	0.75				
0.040	0.00				

Table 1: The quark mass, m , in the Möbius algorithm at fixed $m_\pi = 0.44$. We vary a_5 , M_5 and L_s , one at a time, away from the base case: $(a_5, M_5, L_s) = (1.5, 1.5, 16)$. The dependence on $\alpha = b_5 + c_5$ is not visible to the accuracy quoted above.

4.2 Dependence on a_5 and M_5 at fixed L_s

An exhaustive exploration of the Möbius parameter space M_5, a_5, α for minimizing m_{res} at fixed L_s and m_π is a laborious task. Fortunately it is easy to develop heuristics that simplify the search. Here we describe two limited searches at $L_s = 8$ to illustrate our procedure. These explore the optimization of α for a range of values of a_5 at fixed $M_5 = 1.5$ and subsequently we performed an optimization of M_5 fixing a_5 to its optimal value $a_5 = 1.5$.

In Fig.6 we present the residual mass as defined in Eq. 6.33 for the Möbius operator at $L_s = 8$ and $M_5 = 1.5$, varying a_5 . The series of points for a given a_5 correspond to different values of α . In general, the number of Dirac applications grows with increasing α . But for $a_5 = 1.75$, it can be seen that this behavior changes and it is even reversed at $a_5 = 2.0$. From this graph we conclude that $a_5 = 1.5$ is the optimal point. It gives roughly the same residual mass as the Shamir at $L_s = 16$ with roughly half the Dirac operator applications. To be precise in Fig.6 the values of α are increased by 0.1 moving left to right (for increasing Dirac applications) in the intervals: $\alpha \in [1.0 - 1.3]$ for $a_5 = 0$, $\alpha \in [2.3 - 2.6]$ for $a_5 = 0.75$, $\alpha \in [2.2 - 2.5]$ for $a_5 = 1.0$, $\alpha \in [2.1 - 2.4]$ for $a_5 = 1.25$ and $\alpha \in [1.9 - 2.2]$ for $a_5 = 1.5$. For $a_5 = 2.0$ with the values $\alpha = [1.6, 1.9, 2.0]$, the points reverse direction moving right to left for decreasing Dirac application and for $a_5 = 1.75$ in the cross over region with $\alpha = [1.7 - 2.1]$, the first three points move down to the left and last point moves back to the right.

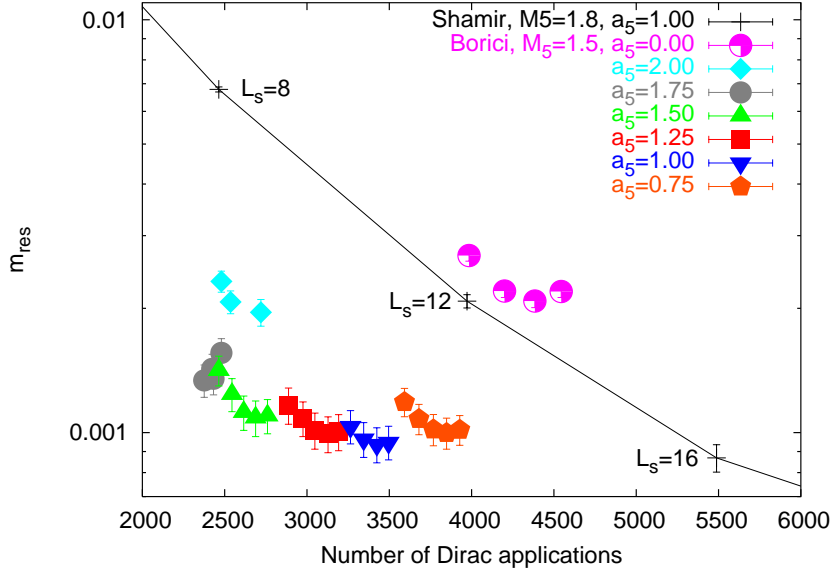


Figure 6: The Möbius algorithm as a function of a_5 and α at fixed pseudoscalar mass, $M_5 = 1.5$ and $L_s = 8$ in comparison with the standard Shamir algorithm of Fig. 4. The series of points for a given a_5 correspond to different values of α enumerated in the text.

Next we fix $a_5 = 1.5$ to its optimal value and explore the M_5 dependence of the residual mass for Möbius action shown in Fig. 7. Here as we increase α in all cases the number of Dirac applications increase. In Fig. 7 moving left to right (for increasing Dirac applications) with neighboring point separated by 0.1 we plotted $\alpha \in [1.6 - 1.9]$ for $M_5 = 1.6$, $\alpha \in [1.9 - 2.2]$ for $M_5 = 1.5$, $\alpha \in [2.3 - 2.6]$ for $M_5 = 1.4$ and $\alpha \in [2.6 - 3.2]$ for $M_5 = 1.3$. It can be seen that $M_5 = 1.5$ and $M_5 = 1.4$ show equally good performance. $M_5 = 1.4$ achieves a little lower residual mass with a corresponding modest increase in the number of Dirac applications. In Fig. 5 summarizing our results for the optimal tuning, we choose $M_5 = 1.5$. Our overall conclusion is that the scaling parameter α is the most important for optimization. This trend is explained in more detail in our discussion of the residual mass in Sec. 6.5 below. We emphasize that if you choose to only minimize the residual mass by increasing α in accordance with the scaling rule in Eq. 2.17 adjusting $\alpha\lambda_{max} < L_s$ for a fixed Möbius kernel, the spectral decomposition of the effective 4d operator is barely modified. So this procedure can be viewed as essentially as an improved algorithm for the same Dirac action, converging more rapidly to the same 4d overlap action in the $L_s \rightarrow \infty$ limit.

Because we performed all our tests at fixed pion mass, one might ask how this opti-

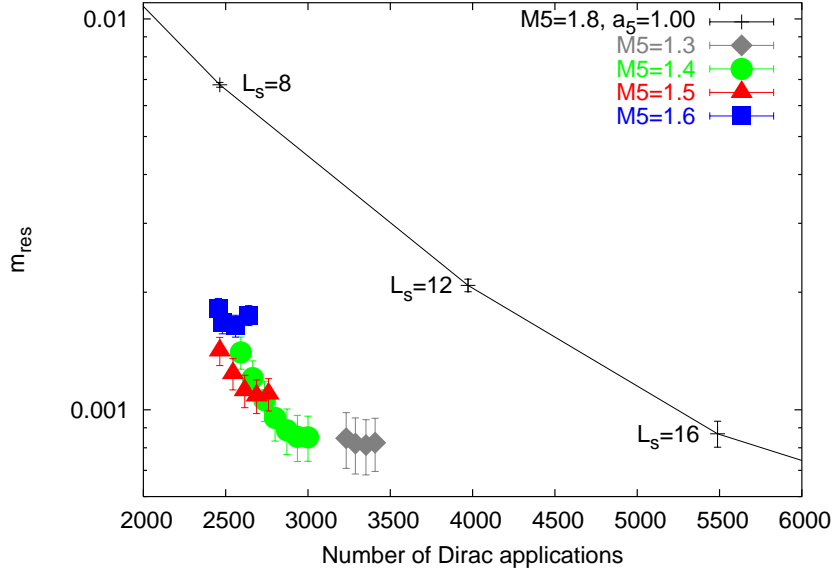


Figure 7: The Möbius algorithm as a function of M_5 and α at fixed pseudo scalar mass, $a_5 = 1.5$ and $L_s = 8$ in comparison with the standard Shamir algorithm of Fig. 4. The series of points for a given M_5 correspond to different values of α enumerated in the text.

mization depends on the bare quark mass. For that reason we repeated our optimization of α at bare quark mass $m = 0.02$ and found that the choices we made in our original test at $m = 0.06$ are still optimal.

4.3 Zolotarev Polynomials for the quenched fields

Finally, we should point out that the Möbius formalism allows for the use of the Zolotarev approximation to the sign function [39, 40] even for $a_5 \neq 0$. One has to introduce an α that is dependent on the fifth dimension. For each 4d slice in the fifth dimension α_s has to be set to the inverse of a root of the Zolotarev polynomial, i.e. for every $s \in L_s$, $\alpha_s = b_s + c_s$ is equal to a Zolotarev coefficient, where $b_s - c_s = a_5$. We define an α (without subscript), as an overall factor, to act as $\alpha * \alpha_s$. In Fig.8 we study the numerical behavior of the Zolotarev approximation, for a setting as shown in Fig.1, i.e. with $L_s = 10$ for Zolotarev and $L_s = 16$ for the polar decomposition, both positioned logarithmically symmetric around one (i.e. per definition with $\alpha = 1$). Fig.8 shows results for $a_5 = 1.0$ and $a_5 = 1.5$. For a given α the residual masses of the two cases agree, as expected from the polynomials in Fig.1. The crucial

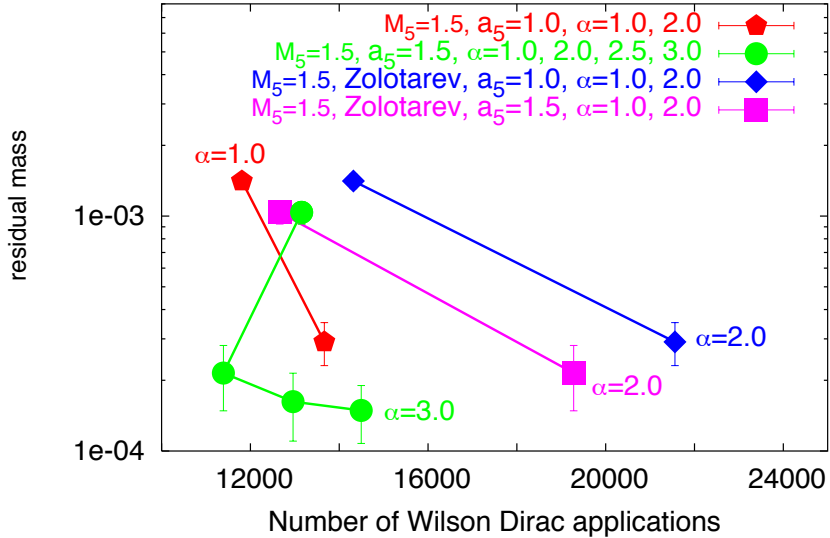


Figure 8: Comparison of the Zolotarev and polar decomposition approximation to the sign function for varying α and two different a_5 .

observation is that for both values of a_5 , the Zolotarev approximation, even though it employs a smaller L_s , required a larger number of Wilson Dirac applications. So far we have not found any way to make Zolotarev competitive to the Möbius in the polar form.

Furthermore, the reflection symmetry and the positivity of the residual mass is lost by using the standard Zolotarev approximation. One can restore these properties by using polynomials with double roots and arranging them in pairs at locations s and $L_s - s - 1$ in the fifth dimension. But the loss of positivity means that m_{res} is no longer be an appropriate measure of chiral symmetry violations. As noted in the introduction a trivial shift in the bare quark mass by m_{res} only cancels the first term in the effective chiral Lagrangian. The higher order terms, such as the clover term, may or may not be improved by the Zolotarev polynomial. Instead for the Zolotarev approximation, a better measure of chiral violation is to consider the sign function, $\Delta(\lambda) = (1 - \epsilon^2(\lambda))/4$, which is uniform across the approximation window $(\lambda_{min}, \lambda_{max})$. If $\Delta(\lambda)$ becomes $\mathcal{O}(\epsilon)$ for all $\lambda \in (\lambda_{min}, \lambda_{max})$, then all chiral properties should be also improved to that order.

5 Domain Wall/Overlap Operator Correspondence

To complete the dictionary between overlap and its corresponding domain implementation, one must show that all Fermionic correlators in a fixed gauge background, $U_\mu(x)$, are equivalent. Namely that

$$\langle \mathcal{O}[q, \bar{q}] \rangle_{DW} = \langle \mathcal{O}[\psi, \bar{\psi}] \rangle_{ov}, \quad (5.1)$$

where here the domain wall correlators are restricted to Dirac fields on the boundaries, (see Fig. 9),

$$q_x = [\mathcal{P}^\dagger \Psi]_{x,s=1} \quad , \quad \bar{q}_x = [\bar{\Psi} D^{DW}(1) \mathcal{P}]_{x,s=1} . \quad (5.2)$$

The Fermionic path integrals $\langle \dots \rangle_{DW}$ and $\langle \dots \rangle_{ov}$ are given by

$$\langle \mathcal{O}[\psi, \bar{\psi}] \rangle_{ov} = \int d\bar{\psi}_x d\psi_x e^{-\bar{\psi}_x D_{x;y}^{ov}(m) \psi_y} \mathcal{O}[\psi, \bar{\psi}], \quad (5.3)$$

and

$$\langle \mathcal{O}[q, \bar{q}] \rangle_{DW} = \int d\bar{\Psi} d\Psi d\bar{\Phi} d\Phi e^{-\bar{\Psi}_{x,s} D_{x,s;y,s}^{DW}(m) \Psi_{y,s'} - \bar{\Phi}_{x,s} D_{x,s;y,s'}^{DW}(1) \Phi_{y,s'}} \mathcal{O}[q, \bar{q}], \quad (5.4)$$

for overlap and domain wall Fermions respectively. In the latter $\bar{\Psi}_{x,s}, \Psi_{x,s}$ are 5d Dirac fields and $\bar{\Phi}_{x,s}, \Phi_{x,s}$ are 5d bosonic Pauli-Villars fields.

Choosing the unit operator $O[q, \bar{q}] = \mathbf{1}$ the lowest order identity is

$$Z_{ov}[U] = Z_{DW}[U], \quad (5.5)$$

choosing the irrelevant field independent overall normalization constant appropriately. This identity is a simple consequence of our ‘‘master’’ equation (5.12) for $K^{DW} = \mathcal{P}^\dagger D_{DW}^{-1}(m) D(1)_{DW} \mathcal{P}$. It is also instructive to see this directly as a field redefinition, $\Phi' = \mathcal{P}^\dagger \Phi$, $\bar{\Phi}' = \bar{\Phi} D^{DW}(1) \mathcal{P}$, in the domain wall partition function. The result is that the Pauli-Villars action is trivial: $\bar{\Phi} D^{DW}(1) \Phi = \bar{\Phi}' \Phi'$. To cancel the Jacobian an identical redefinition is needed for the Dirac field, $Q = \mathcal{P}^\dagger \Psi$, $\bar{Q} = \bar{\Psi} D^{DW}(1) \mathcal{P}$. Thus one can rewrite the domain wall partition function,

$$Z_{DW}[U] = \int d\bar{Q} dQ e^{-\bar{Q} \mathcal{P}^\dagger D^{DW}(1)^{-1} D^{DW}(m) \mathcal{P} Q} = \det(K^{DW}), \quad (5.6)$$

which indicates again why the Dirac matrix, K^{DW} , preconditioned by the Pauli-Villars matrix plays a central role.

Using Wick’s theorem on a general operator establishes the full set of identities. For example Wick’s theorem,

$$\langle q_x \bar{q}_y \rangle_{DW} = [\mathcal{P}^\dagger \underbrace{\Psi \bar{\Psi}}_D D^{DW}(1) \mathcal{P}]_{x_1, y_1} = [\mathcal{P}^\dagger D_{DW}^{-1}(m) D_{DW}(1) \mathcal{P}]_{x_1, y_1} = D_{x,y}^{ov-1}(m),$$

gives the propagator identity,

$$\langle q_x \bar{q}_y \rangle_{DW} = D_{x,y}^{ov-1}(m) = \langle \psi_x \bar{\psi}_y \rangle_{ov} . \quad (5.7)$$

A formal derivation of all Fermionic correlators continues by iteration or more systematically by introducing sources for the Fermion field as a generating function.

In order to avoid confusion it is important to note that our **anti-spinor**,

$$\bar{q}_x = [\bar{\Psi} D^{DW}(1) \mathcal{P}]_{x,s=1} , \quad (5.8)$$

in Eq. 5.2 differs from the traditional choice ⁵,

$$\tilde{q}_x = [\bar{\Psi}(-D_-) \mathcal{R} \mathcal{P}]_{x,s=1} = [\bar{\Psi}(-D_-) \mathcal{P}^\dagger]_{x,s=L_s} = (1-m)^{-1} [\bar{\Psi}(D_{DW}(1) - D_{DW}(m)) \mathcal{P}]_{x,s=1} , \quad (5.9)$$

or $\bar{q}_x = (1-m)\tilde{q}_x + [\bar{\Psi} D_{DW}(m) \mathcal{P}]_{x,s=1}$. The traditional definition results in the awkward subtracted overlap quark propagator

$$\langle q_x \tilde{q}_y \rangle_{DW} = \frac{1}{1-m} [D_{ov}^{-1}(m) - 1]_{xy} . \quad (5.10)$$

Our new definition of \bar{q} smears the boundary field by one lattice unit by virtue of the application of $D^{DW}(1)$ operator. We believe this is a better choice since it simplifies the identities between domain wall and overlap correlation functions, suppressing reference to the particular implementation be it Shamir, Möbius or some future variant. Moreover, an advantage of our definition of \bar{q}_x is that changing the normalization of the operator $D_{DW}(m)$ has **no** effect on the correlation functions since this change cancels with $D_{DW}^{-1}(1)$.

For our discussion of the axial current, it is useful to extend into the bulk both definitions of the anti-spinor, $\bar{Q}_s = [\bar{\Psi} D^{DW}(1) \mathcal{P}]_s$ and $\tilde{Q}_s = [\bar{\Psi}(-D_-) \mathcal{P}^\dagger]_s$ for all s with their respective correlation matrices. These definitions give the following bulk to bulk 5d correlators

$$A_{ss'}^{DW}(m) = \langle Q_s \bar{Q}_{s'} \rangle = [\mathcal{P}^\dagger \frac{1}{D^{DW}(m)} D^{DW}(1) \mathcal{P}]_{s,s'} , \quad (5.11)$$

given in Eq. 2.27 above, and

$$M_{s,s'}(m) = \langle Q_s \tilde{Q}_{s'} \rangle = [\mathcal{P}^\dagger \frac{1}{D^{DW}(m)} (-D_-) \mathcal{P}^\dagger]_{s,s'} , \quad (5.12)$$

respectively. The evaluation of these matrix elements (or correlators) are given in Appendix A. The mass dependence enjoys the nice factorization property, $M^{DW}(m) = A^{DW}(m) M^{DW}(1)$.

⁵In particular $\tilde{q} = [\bar{\Psi} \mathcal{R} \mathcal{P}]_{s=1}$ for the Shamir action with $D_- = -1$.

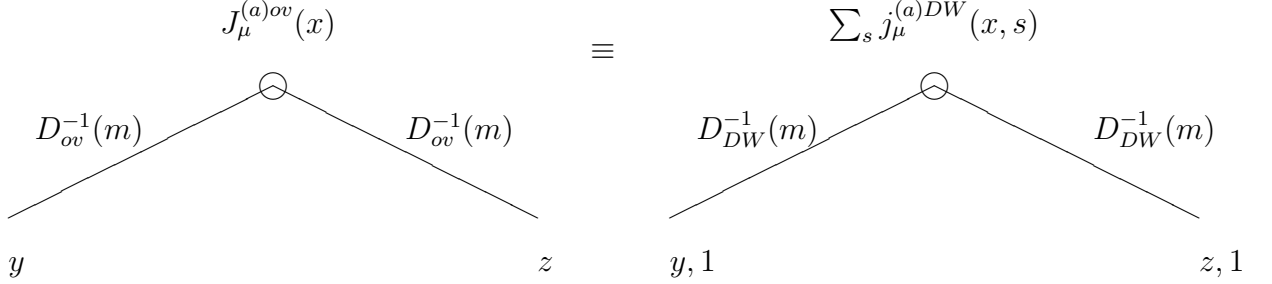


Figure 9: The overlap current insertion in the quark propagator is equivalent to a local 5d current insertion in the domain wall bulk summed over the 5-th co-ordinate s .

5.1 Domain Wall/Overlap correspondence for currents

In the continuum the vector and axial current can be defined by Noether's theorem through the local change of variable in the path integral,

$$\begin{aligned}\psi(x) &\rightarrow \exp[i\theta_V^a(x)\lambda^a + i\theta_A^a(x)\lambda^a\gamma_5] \psi(x) \\ \bar{\psi}(x) &\rightarrow \bar{\psi}(x) \exp[-i\theta_V^a(x)\lambda^a + i\theta_A^a(x)\lambda^a\gamma_5],\end{aligned}\quad (5.13)$$

resulting in Ward identities for the divergence of local currents. The current is then identified after integration by parts. An equivalent method is to *gauge* the action with a flavor gauge field and define the current as the linear response to this gauge field. On the lattice the gauge approach is superior particularly for non-local actions such as the overlap action. For non-local actions, the analog of integration by parts (i.e. *summation by parts*), needed to identify the current in Noether's approach, is difficult to define.

For both the singlet and non-singlet vector current the “gauging” of the action on the lattice action is accomplished by the substitution $U_\mu(x) \rightarrow \exp[i\lambda^a A_\mu^a(x)]U_\mu(x)$ on each link, where $A_\mu^a(x)$ is an adjoint flavor gauge field on link $(x, x + \mu)$. Now by applying the **Domain Wall/Overlap equivalence**, we must have an equivalence between the matrix element for vector and axial currents. From

$$-i\delta_{A_\mu^a(x)} \langle \psi_y^i \bar{\psi}_z^j \rangle_{ov} = -i\delta_{A_\mu^a(x)} \langle q_y^i \bar{q}_z^j \rangle_{DW}, \quad (5.14)$$

we obtain the elegant identity,

$$\langle J_\mu^{(a)ov}(x) \psi_y^i \bar{\psi}_z^j \rangle_{ov} = \langle J_\mu^{(a)DW}(x) q_y^i \bar{q}_z^j \rangle_{DW}, \quad (5.15)$$

neglecting for the moment a contact term that only contributes at $x = z$. The quark flavor indices are labeled by $i, j = 1, \dots, n_f$. The vector current operators resulting from variations of the action are

$$J_\mu^{(a)ov}(x) = -i\delta_{A_\mu^a(x)}\bar{\psi}_y D_{ov}(m)_{y,z}\psi_z = \bar{\psi}\lambda^a V^\mu(x)\psi, \quad (5.16)$$

and

$$J_\mu^{(a)DW}(x) = -i\delta_{A_\mu^a(x)}\bar{\Psi}D_{DW}\Psi + \dots = \bar{\Psi}\lambda^a\mathcal{V}_\mu(x)\Psi + \dots, \quad (5.17)$$

for the overlap and domain wall actions respectively. To derive this is straight forward resulting in

$$\begin{aligned} [D_{ov}^{-1}(m)(\delta_{A_\mu^a(x)}D_{ov}(m))D_{ov}^{-1}(m)]_{yz} &= \langle q_y\bar{\Psi}\rangle_{DW}(\delta_{A_\mu^a(x)}D_{DW})\langle\Psi\bar{q}_z\rangle_{DW} \\ &- \langle Q_y\delta_{A_\mu^a(x)}\bar{q}_z\rangle_{DW}. \end{aligned} \quad (5.18)$$

The last term on the RHS is the contact term due to the dependence of $\bar{q} = [\Psi D^{DW}(m)\mathcal{P}]_1$ on the gauge fields. It only contributes to $x = z$, so it can be ignored except at co-incident points. In the Shamir case the local source $\tilde{q} = [\Psi\mathcal{P}^\dagger]_1$ can be used to avoid this contact term but as described above it then introduces into the propagator a contact term and it is awkward to generalize this to Möbius Fermions. Again as a consistency check, it is worth noting that given the bulk to boundary propagators $\langle q\bar{\Psi}_{s'}\rangle_{DW} = [\mathcal{P}^\dagger D_{DW}^{-1}(1)]_{1s'}$ and $\langle\Psi_s\bar{q}\rangle_{DW} = [D_{DW}^{-1}(m)D_{DW}(1)\mathcal{P}]_{s1}$, discussed in the Appendix A, this identity (5.18) is equivalent to the variational derivative of our fundamental equation (2.28),

$$\delta_{A_\mu^a(x)}D_{ov}^{-1}(m) = \delta_{A_\mu^a(x)}[\mathcal{P}^\dagger\frac{1}{D_{DW}(m)}D_{DW}(1)\mathcal{P}]_{11}, \quad (5.19)$$

including the contact term. This leads to an explicit vector current overlap kernel as a sum over the bulk domain wall modes,

$$V_{yz}^\mu(x) = D_{yy'}^{ov}(m)\langle q_{y'}\bar{\Psi}_{y'',s'}\rangle_{DW}\mathcal{V}^\mu(x)_{y''s',x's}\langle\Psi_{x',s}\bar{q}_{z'}\rangle_{DW}D_{z'z}^{ov}(m). \quad (5.20)$$

Like the overlap propagator itself, this current is non-local in 4d falling off exponential in $|y - x|$ and $|z - x|$. The $+\dots$ in Eq. 5.17 refer to the Pauli-Villars term which does not contribute to the Fermionic matrix element being consider here. However, as we will show later, there are occasions such as conserved current-current correlators, where the Pauli-Villars contribution is **required**. It follows from the identity,

$$\langle J_\mu^{(a)ov}(x)J_\nu^{(b)ov}(y)\rangle = \delta_{A_\mu^a(x)}\delta_{A_\nu^b(y)}\log[Z_{ov}] \equiv \delta_{A_\mu^a(x)}\delta_{A_\nu^b(y)}\log[Z_{DW}], \quad (5.21)$$

that the correlator is

$$\langle J_\mu^{(a)ov}(x)J_\nu^{(b)ov}(y)\rangle = \sum_s \langle j_\mu^{aDW}(x,s)j_\nu^{bDW}(y,s) + j_\mu^{aPV}(x,s)j_\nu^{bPV}(y,s)\rangle, \quad (5.22)$$

as explained in detail in Sec. 6.

Defining the axial current directly from the overlap action is more difficult because the global axial symmetry, which is realized by $\widehat{\gamma}_5 = \gamma_5(1 - D_{ov}(0))$, is non-local and depends on the background gauge field, $U_\mu(x)$. Thus for the axial current we choose to **define** the overlap axial current by imposing the condition,

$$\langle J_\mu^{5(a)ov}(x) \psi_y^i \bar{\psi}_z^j \rangle_{ov} = \langle J_\mu^{5(a)DW}(x) q_y^i \bar{q}_z^j \rangle_{DW} . \quad (5.23)$$

6 Ward-Takahashi Identities

We now proceed to give explicit expressions for the vector and axial current for the Möbius domain wall action. We follow closely the literature in particular the paper of Furman and Shamir [6]. Since the 5d domain action is a function of the 4d Wilson kernel, we begin by reviewing the Wilson vector current to establish notation and useful intermediate kernels. This vector kernel contributes to both the vector and axial current.

Wilson Vector Current: The vector current for Wilson Fermions is well know but let us repeat the argument to establish the notation and methodology for the chiral Fermions. By gauging the Fermions action (2.13) ,

$$S^{Wilson}[U_\mu(x)] = \bar{\Psi} D^{Wilson}[U_\mu(x), M_5] \Psi , \quad (6.1)$$

we compute the first order variation to get the vector current,

$$\mathbb{J}_\mu^a(x) = -i \delta_{A_\mu^a(x)} S^{Wilson}[U_\mu(x) e^{i\lambda^a A_\mu^a(x)}]_{A_\mu^a(x)=0} \equiv \bar{\Psi}_z \mathbb{V}_{zy}^\mu(x) \lambda^a \Psi_y , \quad (6.2)$$

where the ultra local kernel is

$$\mathbb{V}_{zy}^\mu(x) = \frac{\gamma_\mu - 1}{2} U_\mu(x) \delta_{z,x} \delta_{x+\mu,y} + \frac{\gamma_\mu + 1}{2} U_\mu^\dagger(x) \delta_{z,x+\mu} \delta_{x,y} . \quad (6.3)$$

Next we consider the linear responses to change of integration variables, $\Psi_x \rightarrow \exp[i\lambda^a \theta_x^a] \Psi_x$, $\bar{\Psi}_x \rightarrow \bar{\Psi}_x \exp[i\lambda^a \theta_x^a]$ in the path integral and applying Neother's theorem to get a divergence condition of this same current. The change in the action is

$$\begin{aligned} -i \delta_{\theta_x^a} S^{Wilson} &= \bar{\Psi}_x \frac{\gamma_\mu - 1}{2} \lambda^a U_\mu(x) \Psi_{x+\mu} + \bar{\Psi}_{x+\mu} \frac{\gamma_\mu + 1}{2} \lambda^a U_\mu^\dagger(x) \Psi_x - (x \rightarrow x - \mu) \\ &= \mathbb{J}_\mu^a(x) - \mathbb{J}_\mu^a(x - \mu) \equiv \Delta_{-\mu} \mathbb{J}_\mu^a(x) . \end{aligned} \quad (6.4)$$

By Noether theorem we have the lattice current conservation condition, ⁶

$$\sum_{\mu} \mathbb{J}_{\mu}^a(x) - \mathbb{J}_{\mu}^a(x - \mu) \equiv \bar{\Psi}_x \lambda^a \frac{\partial L}{\partial \bar{\Psi}_x} - \frac{\partial L}{\partial \Psi_x} \lambda^a \Psi_x = 0, \quad (6.5)$$

using the classical equations of motion. Actually the divergence condition or Ward-Takahashi identity is a quantum constraint inside the path integral,

$$\langle \Delta_{-\mu} J_{\mu}^a(x) \mathcal{O} \rangle = \langle \delta_{\theta_x^a} \mathcal{O} \rangle, \quad (6.6)$$

which is often given the short hand notation by asserting that, $\Delta_{-\mu} J_{\mu}^a(x) = 0$, is an “operator” equation. If the action or the measure is not invariant additional terms need to be included.

6.1 Domain Wall Vector Current

The derivation of the vector current for the domain wall action parallels the Wilson case closely. Again we gauge the action and take the variation,

$$J_{\mu}^{aDW}(x) = -i\delta_{A_{\mu}^a(x)} \bar{\Psi}_{xs} DDW(m)_{ys,zs'} [U_{\mu}] \Psi_{zs'} - i\delta_{A_{\mu}^a(x)} \bar{\Phi}_{xs} DDW(1)_{ys,zs'} [U_{\mu}] \Phi_{zs'}. \quad (6.7)$$

For the Shamir action the result is

$$J_{\mu}^{aDW}(x) = \sum_{s=1}^{L_s} [\bar{\Psi}_s \lambda^a \nabla^{\mu}(x) \Psi_s + \bar{\Phi}_s \lambda^a \nabla^{\mu}(x) \Phi_s], \quad (6.8)$$

expressed as the Wilson current averaged over all “flavors” in the 5-th direction. The second term involves the Pauli-Villars fields, which give zero contribution to quark correlators. The generalization to the Möbius vector current is straight forward. Taking the variation of the domain wall action in Eq. 2.19 we obtain

$$\begin{aligned} J_{\mu}^{aDW}(x) &= b_5 \sum_{s=1}^{L_s} \bar{\Psi}_s \lambda^a \nabla^{\mu}(x) \Psi_s + c_5 \sum_{s=2}^{L_s} \bar{\Psi}_s \lambda^a \nabla^{\mu}(x) P_+ \Psi_{s-1} + c_5 \sum_{s=1}^{L_s-1} \bar{\Psi}_s \lambda^a \nabla^{\mu}(x) P_- \Psi_{s+1} \\ &- c_5 m (\bar{\Psi}_1 \lambda^a \nabla^{\mu}(x) P_+ \Psi_{L_s} + \bar{\Psi}_{L_s} \lambda^a \nabla^{\mu}(x) P_- \Psi_1) + (\Psi, \bar{\Psi}, m \rightarrow \Phi, \bar{\Phi}, 1). \end{aligned} \quad (6.9)$$

The Pauli-Villars contribution is given exactly by the substitution indicated above. It may seem surprising that the domain wall vector current operator for Möbius Fermions have explicit bare mass dependence but the identity (5.15) with the overlap form requires this. Indeed, in view of

⁶ Of a course “local” currents like gauge variable $U_{\mu}(x)$, on the lattice, $J_{\mu}(x) \equiv J(x, x + \mu)$, are really bilocal variables assigned to a positive links, $(x, x + \mu)$. The current in the negative direction carries the opposite sign: $J(x + \mu, x) \equiv -J_{\mu}(x)$.

the form of the overlap action, $S_F = \bar{\psi} [1 - m] \psi [m / (1 - m) + D_{ov}(0)] \psi$ we see that the effective overlap vector current is independent mass except for the overall factor of $(1 - m)$ which as we mentioned before could be corrected trivially by renormalizing the field by $\sqrt{1 - m}$ and thus removing all mass dependence from the vector current.

An alternative approach to the 4d vector current is to begin with constructing a local 5d conserved vector current,

$$\Delta_{-\mu} j_{\mu}^{aDW}(x, s) + \Delta_{-\hat{5}} j_{\hat{5}}^{aDW}(x, s) = 0 . \quad (6.10)$$

This is accomplished in the same manner as before except now the domain wall action is gauged by a flavor potential, $A_{\mu}^a(x, s)$, depending on the fifth dimension s . The 4d current in Eq. 6.9. is formed by summing over the 5-th axis

$$J_{\mu}^{aDW}(x) = \sum_s j_{\mu}^{aDW}(x, s) , \quad (6.11)$$

and since no current leaks out of the 5-th axis,

$$\sum_s \Delta_{-\hat{5}} j_{\hat{5}}^{aDW}(x, s) = 0 , \quad (6.12)$$

it is conserved as a 4d vector current.

To get the full expression for the 5d vector for Möbius Fermions, we need to take care of off-diagonal terms $D_- P_{\pm}$ by gauging,

$$D_- [U_{\mu}(x)] P_{\mp} \rightarrow D_- [U_{\mu}(x) e^{i\lambda^a A_{\mu}^a(x, s)}] P_{\mp} e^{\pm i\lambda^a A_{\hat{5}}^a(x, s)} . \quad (6.13)$$

The resulting 5d “vector” current $j_M^a(x, s) = j_M^{aDW}(x, s) + j_M^{aPV}(x, s)$ is

$$\begin{aligned} j_{\mu}^{aDW}(x, s) &= b_5 \bar{\Psi}_s \lambda^a \nabla^{\mu}(x) \Psi_s + c_5 \bar{\Psi}_s \lambda^a \nabla^{\mu}(x) P_- \Psi_{s+1} + c_5 \bar{\Psi}_s \lambda^a \nabla^{\mu}(x) P_+ \Psi_{s-1} + \\ &- c_5 (1 + m) \bar{\Psi}_1 \lambda^a \nabla^{\mu}(x) P_+ \Psi_{L_s} \delta_{s,1} + \\ &- c_5 (1 + m) \bar{\Psi}_{L_s} \lambda^a \nabla^{\mu}(x) P_- \Psi_1 \delta_{s,L_s} \end{aligned} \quad (6.14)$$

and

$$\begin{aligned} j_{\hat{5}}^{aDW}(x, s) &= \bar{\Psi}_{x,s} \lambda^a D_- P_- \Psi_{x,s+1} - \bar{\Psi}_{x,s+1} \lambda^a D_- P_+ \Psi_{x,s} + \\ &- (1 + m) \bar{\Psi}_{x,L_s} \lambda^a D_- P_- \Psi_{x,1} \delta_{s,L_s} + \\ &+ (1 + m) \bar{\Psi}_{x,1} \lambda^a D_- P_+ \Psi_{x,L_s} \delta_{s,L_s} . \end{aligned} \quad (6.15)$$

where $s + 1$ is considered modulo L_s . Again the Pauli-Villars current $j_M^{aPV}(x, s)$ takes the same form with substitution $\Psi, \bar{\Psi} \rightarrow \Phi, \bar{\Phi}$ and $m \rightarrow 1$.

6.2 Domain Wall Axial current

The subtlety for the axial current for the domain wall action is that in 5d there is no chirality. The only local current is the 5d vector current defined above. The analog for 4d chirality is the parity transformation that reflects the 5-th axis exchanging the two domain walls. This is the essence of the descent relations [4] that inspired Kaplan's use of the domain construction in the first place.

To implement this on the lattice, one simply splits the extra dimension on any link $(M, M + 1)$ between the two domain walls ($1 < M < L_s - 1$) and defines local vector currents on each side. By gauging each side separately we get a Left current for $s \in [1, M]$ and Right current for $s \in [M + 1, L_s]$. The 4d Ward identities follows from Gauss's law applied to an open interval $s \in [s_0, s_1]$ where the outgoing links $(s_0 - 1, s_0)$ and $(s_1, s_1 + 1)$ on the boundary are dropped – parallel Dirichlet branes if you like. Now flux conservation requires including the flux through these boundaries,

$$\sum_{s=s_0}^{s_1} \Delta_{-\mu} j_{\mu}^a(x, s) = j_5^a(x, s_0 - 1) - j_5^a(x, s_1). \quad (6.16)$$

Although the definition of the axial current can be done using an arbitrary point in the 5th dimension to split the left handed current from the right handed current, we will restrict ourselves to the case where M is taken to be $L_s/2$. Hence, we define the axial (and vector) currents by separating the left and right terms,

$$J_L^{\mu}(x) = \sum_{s=1}^{L_s/2} j_{\mu}^a(x, s) \quad \text{and} \quad J_R^{\mu}(x) = \sum_{s=L_s/2+1}^{L_s} j_{\mu}^a(x, s). \quad (6.17)$$

With periodic boundary condition $J_5^a(x, L_s) - J_5^a(x, 0) = 0$, we have the conserved vector current,

$$J_{\mu}^{aDW}(x) \equiv J_L^{\mu}(x) + J_R^{\mu}(x) = \sum_{s=1}^{L_s} j_{\mu}^a(x, s). \quad (6.18)$$

The odd parity axial current is found by subtraction,

$$J_{DW}^{(5)\mu}(x) = J_L^{\mu}(x) - J_R^{\mu}(x) = \sum_{s=1}^{L_s} \Gamma_5(s - L_s/2) j_{\mu}^a(x, s), \quad (6.19)$$

where $\Gamma_5(s - L_s/2) = \epsilon(L_s/2 + 1/2 - s)$. By Gauss' law we obtain the Ward-Takahashi identity,

$$\Delta_{-\mu} J_{DW}^{(5)\mu}(x) = -2j_5^a(x, L_s) + 2j_5^a(x, L_s/2), \quad (6.20)$$

where

$$\begin{aligned} j_5^a(x, L_s) &= -m \tilde{q}_x \lambda^a \gamma_5 q_x - \tilde{\Phi}_{x, L_s} \gamma_5 \lambda^a \Phi_{x, 1} \\ j_5^a(x, L_s/2) &= \tilde{Q}_{x, L_s/2} \gamma_5 \lambda^a Q_{x, L_s/2+1} + \tilde{\Phi}_{x, L_s/2} \gamma_5 \lambda^a \Phi_{x, L_s/2+1} . \end{aligned} \quad (6.21)$$

6.3 Overlap Axial Current

The remaining task is to use the map between domain wall to overlap Fermions,

$$\langle J_\mu^{5(a)ov}(x) \psi_y^i \bar{\psi}_z^j \rangle_{ov} = \langle J_\mu^{5(a)DW}(x) q_y^i \bar{q}_z^j \rangle_{DW} + i \langle Q_y^i \delta_{A_\mu^a(x)} \bar{q}_z^j \rangle_{DW} , \quad (6.22)$$

to express the divergence in terms of overlap fields. Evaluating

$$\langle \Delta_{-\mu} J_{ov}^{(5)\mu}(x) \psi_y \bar{\psi}_z \rangle_{ov} = \langle (2m \tilde{q}_x \lambda^a \gamma_5 q_x + 2\tilde{Q}_{x,s} \gamma_5 \lambda^a Q_{x,s+1}) q_y \bar{q}_z \rangle_{DW} , \quad (6.23)$$

where $s = L_s/2$, implies,

$$\Delta_{-\mu} J_{ov}^{(5)\mu}(x) = m \bar{\psi}_x [(\gamma_5 + \hat{\gamma}_5) \psi]_x + 2(1-m) \bar{\psi}_z \gamma_5 \rho_{L_s}^{zy}(x) \psi_y , \quad (6.24)$$

as we may readily check. Using the identity: $2\gamma_5 = (1-m)(1 + \gamma_5 \hat{\gamma}_5) + 2D_{ov}(m)$ the first term in Eq. 6.23 gives,

$$\frac{2m}{(1-m)} [D_{ov}^{-1}(m) - 1]_{yx} \gamma_5 [D_{ov}^{-1}(m)]_{xz} = m [D_{ov}^{-1}(m)]_{yx} [(\gamma_5 + \hat{\gamma}_5) D_{ov}^{-1}(m)]_{xz} + \text{CT} , \quad (6.25)$$

where the contact terms (CT) are easily identified as

$$\text{CT} = -\frac{2m}{(1-m)} [\delta_{yx} \gamma_5 D_{ov}^{-1}(m)_{xz} - D_{ov}^{-1}(m)_{yx} \gamma_5 \delta_{x,z}] . \quad (6.26)$$

One may absorb these terms in an appropriate introduction of contact terms in the map from domain wall to axial currents (Eq. 6.22) analogous to those found for the vector current but the procedure is rather arbitrary and unphysical. The second term in Eq. 6.23 is

$$\langle q \tilde{Q}_{x,s+1} \rangle \gamma_5 \langle Q_{x,s} \bar{q} \rangle = (1-m) D_{ov}^{-1}(m) \gamma_5 \Delta_{s+1}^L \Delta_s^R D_{ov}^{-1}(m) , \quad (6.27)$$

where we define the Left and Right breaking term by

$$\Delta_{zx}^L \Delta_{xy}^R = \left[\frac{T_{L_s}^{-1} \dots T_{L_s/2+1}^{-1}}{1 + \mathbb{T}^{-L_s}} \right]_{zx} \left[\frac{T_{L_s/2}^{-1} \dots T_1^{-1}}{1 + \mathbb{T}^{-L_s}} \right]_{xy} \equiv \rho_{L_s}^{zy}(x) , \quad (6.28)$$

whose space-time average $\sum_x \rho_{L_s}(x) = \Delta_{L_s}$ is precisely the correct breaking term for global chiral symmetry found earlier for the overlap action (2.9). In addition note that due to the

conservation of 5d flux, the result is **independent** of the location ($s = L_s/2$) of the mid plane slice. Changing the position merely redefines the axial current by a term with zero total divergence. Nonetheless the natural definition is to take the mid-plane so that parity is equivalent to the reflection operator, $\mathcal{R} : s \rightarrow L_s - s$.

So far we have dealt with the non-singlet sector for the currents. This singlet sector requires some special considerations. In the vector channel one wishes to introduce finite chemical potential for the Baryon number. In the axial channel one needs to show how the axial anomaly arises in the domain wall formalism. In both cases a natural representation in our domain wall/overlap correspondence exists.

6.4 Axial anomaly

The flavor singlet domain wall axial current is anomalous, as has been shown by Kikukawa and Nuguchi [26]. The way this comes about is instructive. This has been computed from the self-contraction of the Fermionic fields, Q and \tilde{Q} , in the bilinear term $\tilde{Q}_{L_s/2}(x)\gamma_5 Q_{L_s/2+1}(x)$ of Eq. 6.23 at the mid-plane of the fifth dimension. This term gives rise both to a contribution to m_{res} (through contraction with the boundary fields) and to a new term that survives in the $L_s \rightarrow \infty$ limit. In order to rigorously perform the calculation, one needs to use the map between domain wall and overlap currents that requires both the domain wall Fermions and the Pauli-Villars “bosons”. The result is that this Fermion contribution at the mid-plane is exactly canceled by the Pauli-Villars contraction and replaced by a boundary contribution at the domain wall. This is really the correct way to understand the physics. For example suppose we modified the domain wall implementation as for example suggest in Ref. [41] by allowing slightly non-uniform gluon fields, $U_\mu(x, s)$, as a function of the fifth coordinate. Without the Pauli-Villars cancellation, the chiral quarks at the boundary would “feel” the wrong gauge potential at the mid-plane giving unphysical and indeed incorrect contributions. This mismatch is cured by the correct calculation.

The calculation proceeds as follows,

$$\begin{aligned} \langle \Delta_\mu J_{DW}^{(5)\mu}(x) \rangle &= 2m \langle \tilde{q}_x \gamma_5 q_x \rangle + 2 \langle \tilde{Q}_{x, L_s/2} \gamma_5 Q_{x, L_s/2+1} \rangle \\ &- 2 \langle \tilde{\Phi}_{x, L_s} \gamma_5 \Phi_{x, 1} \rangle + 2 \langle \tilde{\Phi}_{x, L_s/2} \gamma_5 \Phi_{x, L_s/2+1} \rangle. \end{aligned} \quad (6.29)$$

The first term is the usual quark mass contribution. The second gives two contributions using

the identity

$$\begin{aligned}
-\langle \tilde{Q}_{x,L_s/2} \gamma_5 Q_{x,L_s/2+1} \rangle &= Tr[\gamma_5 A_{L_s/2+1,s}(m) M_{s,L_s/2}(1)]_{x,x} \\
&= (1-m) Tr[\Delta_{L_s/2+1}^R D_{ov}^{-1}(m) \gamma_5 \Delta_{L_s/2}^L]_{x,x} + Tr[\gamma_5 M_{L_s/2+1,L_s/2}(1)]_{x,x},
\end{aligned} \tag{6.30}$$

where $Tr[\dots]$ traces only over color and spin with fixed space time point x . This contributes both a term corresponding the chiral violation for $m_{res} \neq 0$ and a new term which exactly cancels with the mid-term contribution of the Pauli-Villars fields,

$$-\langle \tilde{\Phi}_{x,L_s/2} \gamma_5 \Phi_{x,L_s/2+1} \rangle = -Tr[\gamma_5 M_{L_s/2+1,L_s/2}(1)]_{x,x}. \tag{6.31}$$

The change in sign is due to Bose versus Fermi statistics. Instead now the anomaly comes for the boundary Pauli-Villars term,

$$2\langle \tilde{\Phi}_{x,L_s} \gamma_5 \Phi_{x,1} \rangle = \lim_{m \rightarrow 1} \frac{2}{1-m} Tr[\gamma_5 (D^{ov-1}(m) - 1)]_{x,x} = 2Tr[\gamma_5 (1 - D^{ov}(0))]_{x,x}. \tag{6.32}$$

In the limit of $L_s \rightarrow \infty$, summing over the toroidal volume this gives the lattice Atya-Singer index for the instanton number, $(1/2) \sum_x Tr[\gamma_5 D_{ov}(0)]_{x,x} = n_+ - n_-$. In the continuum limit, Eq. 6.32 gives the topological charge density $(1/32\pi^2) Tr[F_{\mu,\nu}(x) \tilde{F}_{\mu,\nu}(x)]$ as required [48]. The Pauli-Villars term is doing its job by canceling all the heavy cut-off modes in the interior.

6.5 Residual Chiral Violations

At fixed values of L_s the ‘‘residual mass’’ is a common criterion to measure the magnitude of chiral symmetry violations. This is defined in Ref. [36, 38] by the correlator

$$m_{res}(t) = \frac{\sum_{\vec{x}} \langle j_5(\vec{x}, t, L_s/2) j_5(\vec{0}, t, L_s) \rangle_c}{\sum_{\vec{x}} \langle \tilde{q}_{\vec{x},t} \gamma_5 q_{\vec{x},t} \tilde{q}_0 \gamma_5 q_0 \rangle_c} = \frac{\sum_{\vec{x}} \langle \tilde{Q}_{\vec{x},t} \gamma_5 Q_{\vec{x},t} \tilde{q}_0 \gamma_5 q_0 \rangle_c}{\sum_{\vec{x}} \langle \tilde{q}_{\vec{x},t} \gamma_5 q_{\vec{x},t} \tilde{q}_0 \gamma_5 q_0 \rangle_c}, \tag{6.33}$$

in the plateau region with t away from the source and sink. Note however in our definition of m_{res} , we are using our anti-spinors \bar{q} in the denominator that removes the unwanted factor $(1-m)^2$, which of course is irrelevant to the chiral limit ($m = 0$). The fields $\tilde{Q}_{\vec{x},t} = \tilde{Q}_{x,L_s/2}$, $Q_{\vec{x},t} = Q_{x,L_s/2+1}$ are the domain wall fields at the mid-plane link: $(L_s/2, L_s/2 + 1)$. The restriction to connected contributions is a consequence of defining the residual mass via non-singlet pseudoscalar sources which have no disconnected diagram.

Computing the contractions for the connected diagram and using the identities in Sec. A.2 proven in Appendix A for the two point correlators,

$$\gamma_5 \langle q_0 \tilde{Q}_x \rangle \gamma_5 \langle Q_x \tilde{q}_0 \rangle = D_{ov}^{\dagger-1}(0, y) \rho_{L_s}^{yz}(x) D_{ov}^{-1}(z, 0),$$

we have

$$m_{res}(t) = \frac{\sum_{\vec{x}} Tr[\langle q_0 \tilde{Q}_x \rangle \gamma_5 \langle Q_x \tilde{q}_0 \rangle \gamma_5]}{\sum_{\vec{x}} Tr[\langle \bar{q}_x q_0 \rangle \gamma_5 \langle q_x \bar{q}_0 \rangle \gamma_5]} = \frac{\sum_{\vec{x}} Tr[\rho(x) D_{ov}^{-1} D_{ov}^{\dagger-1}]}{\sum_{\vec{x}} Tr[D_{ov}^{-1}(x, 0) D_{ov}^{\dagger-1}(x, 0)]} \simeq \frac{\langle 0 | \bar{q} \gamma_5 \rho(0) q | \pi \rangle}{\langle 0 | \bar{q}_0 \gamma_5 q_0 | \pi \rangle}, \quad (6.34)$$

where,

$$\rho_{L_s}^{zy}(x) = \Delta_{zx}^L \Delta_{xy}^R, \quad (6.35)$$

is defined in Eq. 6.28. The expression on the right in terms of the pion to vacuum matrix element holds for large t separating the source and the sink.

A perhaps less practical but more elegant definition of the residual mass is to sum over all time slices,

$$\bar{m}_{res} = \frac{\sum_{\vec{x}, t} \langle \bar{Q}_{\vec{x}, t} \gamma_5 Q_{\vec{x}, t} \bar{q}_0 \gamma_5 q_0 \rangle_c}{\sum_{\vec{x}, t} \langle \bar{q}_{\vec{x}, t} \gamma_5 q_{\vec{x}, t} \bar{q}_0 \gamma_5 q_0 \rangle_c}, \quad (6.36)$$

resulting in a form,

$$\bar{m}_{res} = \frac{Tr[\Delta_{L_s}(H_5) D_{ov}^{-1} D_{ov}^{\dagger-1}]}{Tr[D_{ov}^{-1} D_{ov}^{\dagger-1}]} = \sum_{\lambda} w_{\pi}(\lambda) \Delta_{L_s}(\lambda) \equiv \langle \Delta_{L_s} \rangle_{\pi}, \quad (6.37)$$

better suited to theoretical analysis. The sum is over the spectrum of the eigenvalues of the transfer matrix. Now the trace includes the sum over the spatial index as well. On the right we introduced the spectral weight for the pion correlator,

$$w_{\pi}(\lambda) = \frac{\langle \lambda | D_{ov}^{-1} D_{ov}^{\dagger-1} | \lambda \rangle}{\sum_{\lambda} \langle \lambda | D_{ov}^{-1} D_{ov}^{\dagger-1} | \lambda \rangle}.$$

In the limit $m \rightarrow 0$, the improved definition \bar{m}_{res} is the normalized trace of the violation of the Ginsparg-Wilson relation written as

$$D_{ov}^{\dagger-1}(0) \Delta_{L_s}(H_5) D_{ov}^{-1}(0) = (D_{ov}^{-1}(0) + \gamma_5 D_{ov}^{-1}(0) \gamma_5 - 2)/2. \quad (6.38)$$

For the polar decomposition the operator Δ_{L_s} is positive definite because the approximation always underestimates the sign function: $|\epsilon_{L_s}(x)| \leq 1$. Consequently, zero residual mass ($m_{res} = 0$) implies the exact Ginsparg-Wilson relations and unbroken Ward-Takahashi relations.

Using this identity (6.37), it is easy to model the residual mass with a reasonable approximation to the spectral density. This model captures well the trends seen in our numerical results in Sec. 4. For the spectral density, $w(\lambda)$, we note that it is plausible that it will have negligible dependences on L_s and α parameterized in terms of unscaled eigenvalues of $H_5 = \gamma_5 D^{Shamir}(M_5)$ so that

$$m_{res} \simeq \sum_{\lambda} w_{\pi}(\lambda) \Delta_{L_s}(\alpha \lambda). \quad (6.39)$$

A simple model for $w_\pi(\lambda)$ is to approximate a few smallest eigenvalues by a finite density $\rho(0)$ due to “small topological defects” and at larger eigenvalues by the free kernel. Indeed this ansatz is able to give a good fit to our empirical study of the parameter dependence of m_{res} in Sec. 4.

At large L_s the defect dominate the contribution to m_{res} . Using the expression $\epsilon_{L_s}(\alpha\lambda) = \tanh(x)$ with $x = L_s \log(1 + \alpha\lambda) - L_s \log(1 - \alpha\lambda)$ we get the expression for the error

$$\Delta_{L_s}(\alpha\lambda) = 1/(4 \cosh^2(x)) \rightarrow e^{-L_s |\log(1 + \alpha\lambda) - \log(1 - \alpha\lambda)|}, \quad (6.40)$$

for $O(L_s^{-1}) < |\alpha\lambda| < O(L_s)$. Outside this window the error is $O(1)$. For large L_s the error is dominated by the small eigenvalues in the interval $|\lambda| < 1/(\alpha L_s)$. For the standard Shamir form ($\alpha = 1$) this causes the residual to fall like $m_{res} \sim \rho(0)/L_s$ asymptotically but for the rescaled Möbius with $\alpha \sim L_s/\lambda_{max}$ we estimate the residual to fall like $m_{res} \sim \rho(0)/L_s^2$ asymptotically⁷. This improvement is, we believe, the basic explanation for the superior chirality of the Möbius algorithm.

As we mentioned above, the polar approximation to the sign function results in a positive residual mass. However, other polynomial approximations, such as Zolotarev, of the sign function may oscillate around $\epsilon(x)$ so positivity is lost. In fact one can even “tune” m_{res} to zero but this does **not** imply that chiral symmetry is exact. Instead it implies that the lowest order dimension 3 operator in to the chiral Lagrangian is given by the quark mass. The real issue is higher order terms, in particular the dimension 5 chiral symmetry breaking operators.

6.6 Baryon current and Chemical Potential

The chemical potential couples to the singlet charge of the vector current, i.e. Baryon number. In this section we point out the relation of the vector current we already defined to the non-zero chemical potential formulation of the overlap and domain wall Fermions. It is useful to note that the same strategy can be used to define currents for kernels that violate γ_5 Hermiticity leading to complex determinants such as the Dirac operator with a chemical potential. Block and Wettig [49] have given the overlap operator for non-zero chemical potential. Their construction is tricky because of the need to define the “sign function” for a non-Hermitian kernel “ $\epsilon(A)$ ”,

⁷Strictly speaking one should be careful about the order of limits. The eigenvalue distribution is only properly given by a density function, $\rho(\lambda)$, in the limit of infinite lattice volume (L^4), so here at finite volume $\rho(0)$ should be replaced by a measure of the mean number of eigenvalues in the interval near $\lambda = 0$ where the exponential approximation to $\epsilon(\lambda)$ fails. At fixed volume, L^4 , exponential convergence to $m_{res} = 0$ is expected to resume for $L_s \gg L$ but this is of little practical importance.

where $A = \gamma_5 D^{Wilson}(M_5, \mu)$ is given by making the standard substitution for non-zero chemical potential,

$$(1 \pm \gamma_4)U_{\pm 4}(x) \rightarrow (1 \pm \gamma_4)e^{\pm \mu}U_{\pm 4}(x) \quad (6.41)$$

into the Wilson operators for all time like links. Their rule is to define the “sign function” by

$$“\epsilon(A)” = S \text{sign}(Re \Lambda) S^{-1}, \quad (6.42)$$

where S is the similarity transformation that diagonalizes the kernel $A = SAS^{-1}$.

It is straight forward to rederive their prescription and generalize it for any kernel at finite L_s by simply inserting this Wilson operator (for non-zero μ) into our generalized domain wall formalism. In the domain wall form we get,

$$\epsilon_{L_s}(A) = \frac{T^{-L_s} - 1}{T^{-L_s} + 1} = \frac{(1 + A)^{L_s} - (1 - A)^{L_s}}{(1 + A)^{L_s} + (1 - A)^{L_s}} = S \frac{(1 + \Lambda)^{L_s} - (1 - \Lambda)^{L_s}}{(1 + \Lambda)^{L_s} + (1 - \Lambda)^{L_s}} S^{-1}, \quad (6.43)$$

where we diagonalize $A = SAS^{-1}$ with eigenvalues $\lambda = x + iy$. As shown in Appendix A, $A = (T^{-1} + 1)^{-1}(T^{-1} - 1) = \gamma_5(D_+ + D_-)/[\gamma_5(D_+ - D_-)\gamma_5]$ or $A = \gamma_5 D_W(\mu)$ for Boriçi. But using $|(1 \pm \lambda)^{L_s}| = |1 \pm \lambda|^{L_s}$ or $|(1 \pm x \pm iy)^{L_s}| = [(1 \pm x)^2 + y^2]^{L_s/2}$ we see that the exponentially dominant of the two terms for each eigenvalue is the one where the sign of $\pm x$ is positive. Hence we get

$$\epsilon_{L_s}(A) \rightarrow S \text{sign}(Re \Lambda) S^{-1}, \quad (6.44)$$

in **exact** agreement with Block and Wettig at $L_s = \infty$.

7 Conclusions

In this paper we have reviewed the Möbius class of chiral domain wall Fermion operators [17, 18]. Since they are just now coming into wider use in production codes, a general presentation of the formalism is perhaps warranted. We have sought to emphasize several features critical to their performance and chiral properties. On the performance side, we note that the Möbius kernel operator requires no additional applications of the 4-d Wilson Dirac kernel per domain wall iteration. However we are required to replace the conventional 5-d red-black preconditioning by a 4-d checkerboard with constant color in the 5-th axis in order to avoid a 4-d Wilson operator inverse as a new inner loop. In fact such 4-d even/odd decomposition is needed for the earlier Boriçi domain wall formulation [27, 28], as well as any operator that goes beyond nearest neighbor terms in the 5-th direction. A highly optimized parallel Möbius Domain Wall Fermion (MDWF) inverter for clusters and the Blue Gene architecture has been freely available for several years [21] as well as Hybrid Monte Carlo evolution code in Chroma [50]. Very soon the Möbius inverters will be available in the QUDA [51] (QCD in CUDA) library for NVIDIA multi-GPUs platforms as well as a full Hybrid Monte Carlo evolution code in the Columbia Physics System [52] (CPS) for Möbius fermions optimized for the BlueGene/Q.

In addition, in this paper we worked out the form of the conserved and partially conserved axial vector currents for Möbius domain wall fermions, as well as their Ward-Takahashi identities. The goal was to have a general approach that maps the domain wall expressions at finite L_s into their equivalent form for the effective 4-d overlap action. A byproduct of our formalism is a simple derivation of the overlap operator at finite chemical potential, a result first obtained by Block and Wettig [49]. Also we show how the general expression for the residual mass, in the case of non-vanishing zero mode density, implies quadratic convergence, $m_{res} = O(1/L_s^2)$, for the appropriately scaled Möbius fermions for large L_s in contrast to the slower linear convergence, $m_{res} = O(1/L_s)$, for Shamir. This largely explains the reason for the improved chiral behavior of the Möbius rescaling algorithm. Indeed, for the test ensemble we used, our numerical tests support this picture and even suggest that Möbius at $L_s = 32$ should correspond roughly to running Shamir with $L_s = O(10^3)$. Of course the latter is neither practical or even easily amenable to direct numerical verification.

Perhaps of more interest is to consider using the Möbius algorithm to reduce L_s substantially. For new HMC runs, one can be even more aggressive. For example as illustrated in Fig. 10, the typical simulation with Shamir at $L_s = 16$ might be run with Möbius at L_s as low as $L_s = 4$ with a tolerable compromise on chirality. Perhaps not all simulations can be this aggressive but there may be some that can. For example exploratory investigations for Beyond

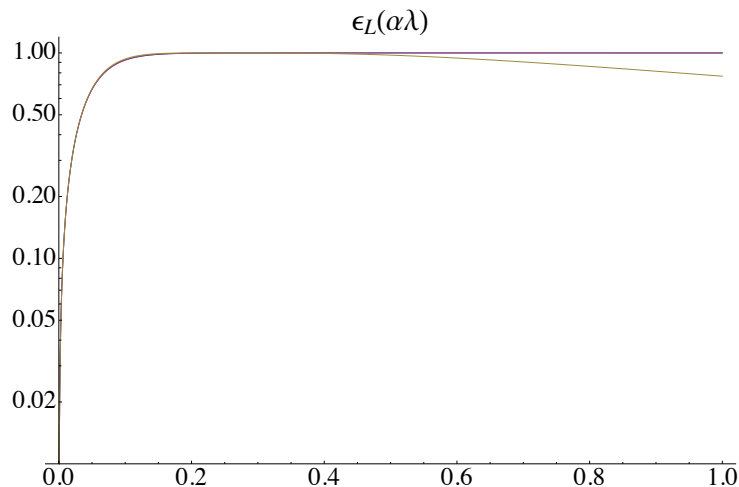


Figure 10: Comparison the approximate of the sign function $\epsilon_{L_s}(\alpha\lambda)$ plotted against λ for Shamir ($\alpha = 1$) at $L_s = 16$ with rescaled Möbius ($\alpha = 2$) at $L_s = 8$ (indistinguishable) and the lower curve scaled Möbius ($\alpha = 4$) at $L_s = 4$. The support for the kernel is bounded by eigenvalues $|\lambda| < (8 - M_5)/(10 - M_5) \simeq 0.75$ so the visible degradation at the top is limited and should not be significant for the chiral physics at small eigenvalue.

the Standard Model (BSM) physics might try this at least in early broad surveys of the gauge theory landscape.

We are also aware that as the Möbius algorithm comes into more common use, there are potentially opportunities to combine it with other algorithmic methods such as Hasenbusch [53] mass precondition or multigrid preconditioning [23, 22]. For the latter it is interesting to note that the first level of domain wall multigrid maps the 5-d operator into an effective 4-d coarse operator [24] suggesting many avenues of investigations that could allow domain wall codes to compete favorably with 4-d Wilson codes. One example of a hybrid algorithm that has received some preliminary investigation is combining the Möbius algorithm with the idea of Gap Fermions [54] to further reduce the value of m_{res} at fixed L_s as noted in Fig. 11 reproduced from Ref. [19]. The figure shows that the smoothing consequences of introducing a Gapped action can further reduce the residual mass by as much as an order of magnitude for $L_s = 16$ for example.

The interaction between different algorithmic methods opens up a large range of possible improvements worth of serious study. The RBC collaboration has been pursuing similar strategies [55], to try to balance the apparently conflicting desire for better chirality while still facilitating sufficient thermalization of topological charge sectors. We have no magic solution

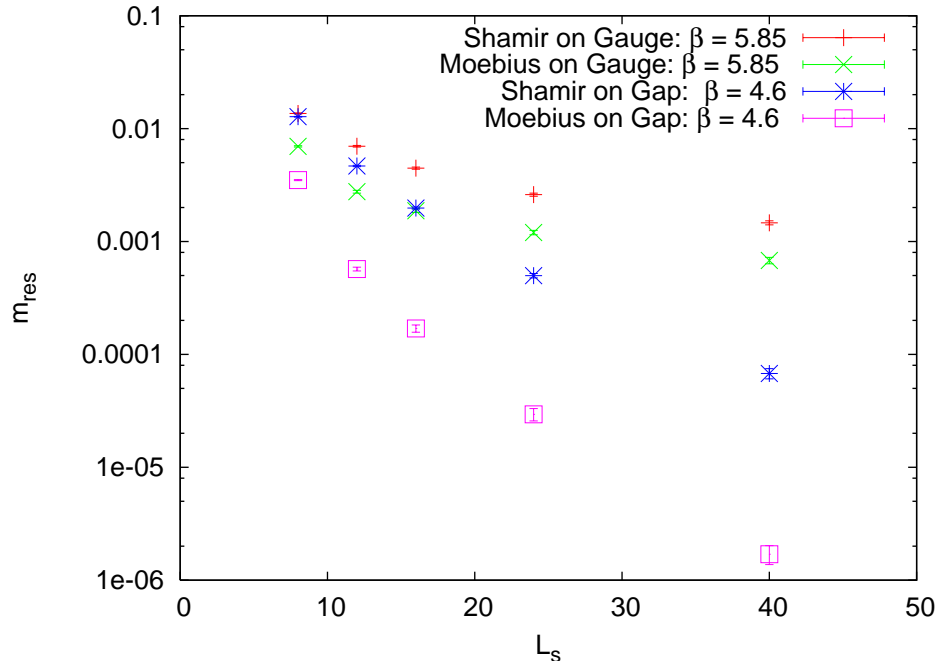


Figure 11: The Möbius algorithm ($\alpha = 2$) on pure gauge and Gap lattices vs Shamir ($\alpha = 1$).

to this but of course the interaction of Möbius fermions with other algorithmic approaches begs further explorations in this endeavor.

Acknowledgment: We wish to acknowledge many useful discussions and interactions with Andrew Pochinsky, Claudio Rebbi, David Schaich and Pavlos Vranas. This research was supported in part at William and Mary by DOE grant DE-FG02-07ER41527 and by DE-AC05-06OR23177 (JSA), and in part at Boston University by U.S. DOE grants DE-FG02-91ER40676 and DE-FC02-06ER41440; NSF grants DGE-0221680, PHY-0427646, and PHY-0835713.

References

- [1] Holger B. Nielsen and Masao Ninomiya. Absence of neutrinos on a lattice. 1. proof by homotopy theory. *Nucl. Phys.*, B185:20, 1981.
- [2] Holger B. Nielsen and Masao Ninomiya. Absence of neutrinos on a lattice. 2. intuitive topological proof. *Nucl. Phys.*, B193:173, 1981.
- [3] David B. Kaplan. A method for simulating chiral fermions on the lattice. *Phys. Lett.*, B288:342–347, 1992.
- [4] Curtis G. Callan and Jeffrey A. Harvey. Anomalies and fermion zero modes on strings and domain walls. *Nucl. Phys.*, B250:427, 1985.
- [5] Yigal Shamir. Chiral fermions from lattice boundaries. *Nucl. Phys.*, B406:90–106, 1993.
- [6] Vadim Furman and Yigal Shamir. Axial symmetries in lattice qcd with kaplan fermions. *Nucl. Phys.*, B439:54–78, 1995.
- [7] Rajamani Narayanan and Herbert Neuberger. Infinitely many regulator fields for chiral fermions. *Phys. Lett.*, B302:62–69, 1993.
- [8] Rajamani Narayanan and Herbert Neuberger. Chiral fermions on the lattice. *Phys. Rev. Lett.*, 71:3251–3254, 1993.
- [9] Rajamani Narayanan and Herbert Neuberger. Chiral determinant as an overlap of two vacua. *Nucl. Phys.*, B412:574–606, 1994.
- [10] Herbert Neuberger. Vector like gauge theories with almost massless fermions on the lattice. *Phys. Rev.*, D57:5417–5433, 1998.
- [11] Herbert Neuberger. Exactly massless quarks on the lattice. *Phys. Lett.*, B417:141–144, 1998.
- [12] Paul H. Ginsparg and Kenneth G. Wilson. A remnant of chiral symmetry on the lattice. *Phys. Rev.*, D25:2649, 1982.
- [13] P. Hasenfratz. Prospects for perfect actions. *Nucl. Phys. Proc. Suppl.*, 63:53–58, 1998.
- [14] Wolfgang Bietenholz and U.J. Wiese. Perfect lattice actions for quarks and gluons. *Nucl.Phys.*, B464:319–352, 1996.
- [15] Wolfgang Bietenholz, R. Brower, S. Chandrasekharan, and U.J. Wiese. Progress on perfect lattice actions for QCD. *Nucl.Phys.Proc.Suppl.*, 53:921–934, 1997.

- [16] Martin Luscher. Exact chiral symmetry on the lattice and the ginsparg-wilson relation. *Phys. Lett.*, B428:342–345, 1998.
- [17] Richard C. Brower, Hartmut Neff, and Kostas Orginos. Mobius fermions: Improved domain wall chiral fermions. *Nucl.Phys.Proc.Suppl.*, 140:686–688, 2005.
- [18] R.C. Brower, H. Neff, and K. Orginos. Mobius fermions. *Nucl.Phys.Proc.Suppl.*, 153:191–198, 2006.
- [19] Richard Brower, Ron Babich, Kostas Orginos, Claudio Rebbi, David Schaich, et al. Moebius Algorithm for Domain Wall and GapDW Fermions. *PoS, LATTICE2008:034*, 2008.
- [20] Hantao Yin and Robert D. Mawhinney. Improving DWF Simulations: the Force Gradient Integrator and the Mobius Accelerated DWF Solver. *PoS, LATTICE2011:051*, 2011.
- [21] Andrew Pochinsky. Writing efficient QCD code made simpler: QA(0). *PoS, LATTICE2008:040*, 2008. See <http://www.mit.edu/~avp/mdwf/>.
- [22] Ronald Babich, James Brannick, Richard C. Brower, Michael A. Clark, Saul D. Cohen, J. C. Osborn, and C. Rebbi. The Role of multigrid algorithms for LQCD. *PoS, LAT2009:031*, 2009.
- [23] R. Babich, J. Brannick, R.C. Brower, M.A. Clark, T.A. Manteuffel, S. F. McCormick, J. C. Osborn, and C. Rebbi. Adaptive multigrid algorithm for the lattice Wilson-Dirac operator. *Phys.Rev.Lett.*, 105:201602, 2010.
- [24] Saul D. Cohen, R.C. Brower, M.A. Clark, and J.C. Osborn. Multigrid Algorithms for Domain-Wall Fermions. *PoS, LATTICE2011:030*, 2011.
- [25] Robert G. Edwards, Urs M. Heller, and Rajamani Narayanan. Approach to the continuum limit of the quenched hermitian wilson-dirac operator. *Phys. Rev.*, D60:034502, 1999.
- [26] Yoshio Kikukawa and Tatsuya Noguchi. Low energy effective action of domain-wall fermion and the ginsparg-wilson relation. [hep-lat/9902022](http://arxiv.org/abs/hep-lat/9902022), 1999.
- [27] Artan Borici. Truncated overlap fermions: The Link between overlap and domain wall fermions (*in Lattice fermions and structure of the vacuum, V. K. Mitrjushkin and G. Schierholz (eds)*). pages 41–52, 1999.
- [28] A. Borici. Truncated overlap fermions. *Nucl.Phys.Proc.Suppl.*, 83:771–773, 2000.
- [29] Ardan Borici, Andreas Frommer, Balint Joo, Kennedy Anthony D., and Pendleton Brian. *QCD and numerical analysis*. Springer, 2005.

- [30] Alban Allkoci and Artan Borici. Reducing the beta-shift in domain wall fermion simulations. *PoS*, LAT2005:099, 2006.
- [31] Michael Cheng et al. The finite temperature QCD using 2+1 flavors of domain wall fermions at $N_t = 8$. *Phys. Rev.*, D81:054510, 2010.
- [32] Joel Giedt, Richard Brower, Simon Catterall, George T. Fleming, and Pavlos Vranas. Lattice super-Yang-Mills using domain wall fermions in the chiral limit. *Phys. Rev.*, D79:025015, 2009.
- [33] Pavlos M. Vranas. Chiral symmetry restoration in the schwinger model with domain wall fermions. *Phys. Rev.*, D57:1415–1432, 1998.
- [34] Robert G. Edwards and Urs M. Heller. Domain wall fermions with exact chiral symmetry. *Phys. Rev.*, D63:094505, 2001.
- [35] A.D. Kennedy. Algorithms for dynamical fermions. hep-lat/0607038, 2006.
- [36] T. Blum et al. Quenched lattice qcd with domain wall fermions and the chiral limit. *Phys. Rev.*, D69:074502, 2004.
- [37] A. Ali Khan et al. Chiral properties of domain-wall quarks in quenched qcd. *Phys. Rev.*, D63:114504, 2001.
- [38] Y. Aoki et al. Domain wall fermions with improved gauge actions. *Phys. Rev.*, D69:074504, 2004.
- [39] Ting-Wai Chiu. Optimal domain-wall fermions. *Phys. Rev. Lett.*, 90:071601, 2003.
- [40] Ting-Wai Chiu. Locality of optimal lattice domain-wall fermions. *Phys. Lett.*, B552:97–100, 2003.
- [41] Oliver Bar, Rajamani Narayanan, Herbert Neuberger, and Oliver Witzel. Domain wall filters. hep-lat/0703013, 2007.
- [42] David B. Kaplan and Martin Schmaltz. Supersymmetric Yang-Mills theories from domain wall fermions. *Chin.J.Phys.*, 38:543–550, 2000.
- [43] Taku Izubuchi. Lattice QCD with dynamical domain wall quarks. *Nucl.Phys.Proc.Suppl.*, 119:813–815, 2003.
- [44] D.J. Antonio et al. First results from 2+1 Flavor Domain Wall QCD: Mass Spectrum, Topology Change and Chiral Symmetry with $L(s) = 8$. *Phys.Rev.*, D75:114501, 2007.

- [45] Yigal Shamir. New domain wall fermion actions. *Phys.Rev.*, D62:054513, 2000.
- [46] Maarten Golterman, Yigal Shamir, and Benjamin Svetitsky. Localization properties of lattice fermions with plaquette and improved gauge actions. *Phys.Rev.*, D72:034501, 2005.
- [47] David J. Antonio et al. Localization and chiral symmetry in three flavor domain wall QCD. *Phys.Rev.*, D77:014509, 2008.
- [48] Ferenc Niedermayer. Exact chiral symmetry, topological charge and related topics. *Nucl. Phys. Proc. Suppl.*, 73:105–119, 1999.
- [49] Jacques Bloch and Tilo Wettig. Overlap dirac operator at nonzero chemical potential and random matrix theory. *Phys. Rev. Lett.*, 97:012003, 2006.
- [50] Robert G. Edwards and Balint Joo. The Chroma software system for lattice QCD. *Nucl.Phys.Proc.Suppl.*, 140:832, 2005.
- [51] M.A. Clark, R. Babich, K. Barros, R.C. Brower, and C. Rebbi. Solving Lattice QCD systems of equations using mixed precision solvers on GPUs. *Comput.Phys.Commun.*, 181:1517–1528, 2010. See <http://lattice.github.com/quda/>.
- [52] The columbia physics system (cps). <http://www2.epcc.ed.ac.uk/ukqcd/tcc/>.
- [53] Martin Hasenbusch. Speeding up the hybrid Monte Carlo algorithm for dynamical fermions. *Phys.Lett.*, B519:177–182, 2001.
- [54] Pavlos M. Vranas. Gap Domain Wall Fermions. *Phys.Rev.*, D74:034512, 2006.
- [55] Christopher Kelly. Continuum Results for Light Hadronic Quantities using Domain Wall Fermions with the Iwasaki and DSDR Gauge Actions. *PoS, LATTICE2011:285*, 2011.

A Möbius generalization of Domain Wall Operator

This appendix collects together the basic identities that relate our generalized domain wall operator at finite L_s to the effective operators in the 4d overlap world. The class of domain wall operator (including our Möbius and Zolotarev cases) has next to nearest neighbor interaction in the fifth axis,

$$\begin{aligned} D_{DW}(m)_{s,s'} &= D_-^{(s)} P_+ \delta_{s,s'+1} + D_+^{(s)} \delta_{s,s'} + D_-^{(s)} P_- \delta_{s,s'-1} \\ &\quad - m D_-^{(1)} P_+ \delta_{s,1} \delta_{s',L_s} - m D_-^{(L_s)} P_- \delta_{s,L_s} \delta_{s',1}, \end{aligned} \quad (\text{A.1})$$

with $s, s' = 1, 2, \dots, L_s \bmod L_s$ cyclic moduls L_s and $P_\pm = \frac{1}{2}(1 \pm \gamma_5)$ and $D_+^{(s)} = b_5(s) D^{Wilson}(M_5) + 1$, $D_-^{(s)} = c_5(s) D^{Wilson}(M_5) - 1$. The Wilson operator is

$$D_{xy}^{Wilson}(M_5) = (4 + M_5) \delta_{x,y} - \frac{1}{2} \left[(1 - \gamma_\mu) U_\mu(x) \delta_{x+\mu,y} + (1 + \gamma_\mu) U_\mu^\dagger(y) \delta_{x,y+\mu} \right]. \quad (\text{A.2})$$

In matrix notation the domain wall operator is

$$D_{DW}(m) = \begin{bmatrix} D_+^{(1)} & D_-^{(1)} P_- & 0 & \cdots & -m D_-^{(1)} P_+ \\ D_-^{(2)} P_+ & D_+^{(2)} & D_-^{(2)} P_- & \cdots & 0 \\ 0 & D_-^{(3)} P_+ & D_+^{(3)} & \cdots & 0 \\ \vdots & \vdots & \vdots & \ddots & \vdots \\ -m D_-^{(L_s)} P_- & 0 & 0 & \cdots & D_+^{(L_s)} \end{bmatrix}. \quad (\text{A.3})$$

We will also on occasion discuss the equally valid “left” form

$$\widehat{D}_{DW}(m) = D_-^{-1} D_{DW}(m) D_-, \quad (\text{A.4})$$

with $D_- = \text{Diag}[D_-^{(1)}, D_-^{(2)}, D_-^{(2)}, \dots, D_-^{(L_s)}]$, which rotates the chiral projectors to the left,

$$\widehat{D}_{DW}(m) = \begin{bmatrix} D_+^{(1)} & P_- D_-^{(2)} & 0 & \cdots & -m P_+ D_-^{(L_s)} \\ P_+ D_-^{(1)} & D_+^{(2)} & P_- D_-^{(3)} & \cdots & 0 \\ 0 & P_+ D_-^{(2)} & D_+^{(3)} & \cdots & 0 \\ \cdots & \cdots & \cdots & \cdots & \cdots \\ -m P_- D_-^{(1)} & 0 & 0 & \cdots & D_+^{(L_s)} \end{bmatrix}, \quad (\text{A.5})$$

because of its possible advantage for efficient code.

A.1 LDU decomposition

To relate the 5d domain wall matrix to the 4 dimensional overlap form, one merely performs a standard **LDU decomposition** of Eq. A.3, although the notation in the domain wall literature

(which we adhere to here) is unconventional and obscures this a bit. Consider the decomposition,

$$D_{DW}\mathcal{P} = "UDL" . \quad (\text{A.6})$$

The interchange of U and L relative to conventions of mathematics texts is inconsequential since reflecting the 5-th axis with transformation, \mathcal{R} defined in Eq. 2.23 converts any U matrix to an L matrix and vice versa.

The first step is to multiply by the permutation (or pivot) matrix that performs a left shift C for positive chirality components:

$$\mathcal{P} = P_-I + P_+C = \begin{bmatrix} P_- & P_+ & 0 & \cdots & 0 \\ 0 & P_- & P_+ & \cdots & 0 \\ 0 & 0 & P_- & \cdots & 0 \\ \cdots & \cdots & \cdots & \cdots & \cdots \\ P_+ & 0 & 0 \cdots & & P_- \end{bmatrix} . \quad (\text{A.7})$$

With $Q_-^{(s)} = \gamma_5[D_-^{(s)}P_+ + D_+^{(s)}P_-]$ and $Q_+^{(s)} = \gamma_5[D_+^{(s)}P_+ + D_-^{(s)}P_-]$, this gives an upper diagonal form:

$$D_{DW}(m)\mathcal{P} = \gamma_5 \begin{bmatrix} Q_-^{(1)}c_- & Q_+^{(1)} & 0 & \cdots & 0 \\ 0 & Q_-^{(2)} & Q_+^{(2)} & \cdots & 0 \\ 0 & 0 & Q_-^{(3)} & \cdots & 0 \\ \vdots & \vdots & \vdots & \ddots & \vdots \\ Q_+^{(L_s)}c_+ & 0 & 0 & \cdots & Q_-^{(L_s)} \end{bmatrix} , \quad (\text{A.8})$$

or,

$$D_{DW}(m)\mathcal{P} = \gamma_5 Q_- \begin{bmatrix} c_- & -T_1^{-1} & 0 & \cdots & 0 \\ 0 & 1 & -T_2^{-1} & \cdots & 0 \\ 0 & 0 & 1 & \cdots & 0 \\ \vdots & \vdots & \vdots & \ddots & \vdots \\ -T_{L_s}^{-1}c_+ & 0 & 0 & \cdots & 1 \end{bmatrix} , \quad (\text{A.9})$$

after factoring out the the diagonal matrix, $Q_- = \text{Diag}[Q_-^{(1)}, Q_-^{(2)}, \dots, Q_-^{(L_s)}]$. Here we define the mass dependent constants, $c_{\pm} = P_{\pm} - mP_{\mp} = \frac{1}{2}(1 - m) \pm \frac{1}{2}(1 + m)\gamma_5$, and the 4d local "transfer matrix", $T_{[s+1,s]} \equiv T_s$, from s to $s+1$ on the $[s+1, s]$ or in fact its inverse,

$$T_{[s,s+1]} \equiv T_s^{-1} = -(Q_-^{(s)})^{-1}Q_+^{(s)} . \quad (\text{A.10})$$

This operator is Hermitian and relates to a 5d s dependent Hamiltonian operator by the identity,

$$H_s = \frac{T_s^{-1} - 1}{T_s^{-1} + 1} = \frac{1}{Q_+^s - Q_-^s} (Q_+^s + Q_-^s) = \gamma_5 \frac{D_+^{(s)} + D_-^{(s)}}{D_+^{(s)} - D_-^{(s)}} . \quad (\text{A.11})$$

Thus we have an s dependent version of the Möbius operators given in Eq. 2.14,

$$H_s = \gamma_5 \frac{(b_5(s) + c_5(s))D^{Wilson}(M_5)}{2 + (b_5(s) - c_5(s))D^{Wilson}(M_5)}. \quad (\text{A.12})$$

The remaining two steps are Gaussian elimination with “U” and back substitution with “L”, to obtain ⁸

$$D_{DW}(m) \mathcal{P} = \gamma_5 Q_- U D_5(m) L(m), \quad (\text{A.13})$$

in terms of

$$U = \begin{bmatrix} 1 & -T_1^{-1} & 0 & \cdots & 0 \\ 0 & 1 & -T_2^{-1} & \cdots & 0 \\ 0 & 0 & 1 & \cdots & 0 \\ \vdots & \vdots & \vdots & \ddots & \vdots \\ 0 & 0 & 0 & \cdots & 1 \end{bmatrix} \quad L(m) = \begin{bmatrix} -1 & 0 & 0 & \cdots & 0 \\ -T_{[2,1]}c_+ & 1 & 0 & \cdots & 0 \\ -T_{[3,1]}c_+ & 0 & 1 & \cdots & 0 \\ \vdots & \vdots & \vdots & \ddots & \vdots \\ -T_{[L_s,1]}c_+ & 0 & 0 & \cdots & 1 \end{bmatrix}, \quad (\text{A.14})$$

where $T_{[s,1]} = T_s^{-1}T_{s+1}^{-1} \cdots T_{L_s}^{-1}$, assuming periodic index notation $1 = \mathbf{mod} L_s + 1$. For future reference this notation is generalized to s -ordered products ($1 \leq s < s' \leq L_s$),

$$T_{[s,s'+1]} = T_s^{-1}T_{s+1}^{-1} \cdots T_{s'}^{-1} \quad , \quad T_{[s'+1,s]} = T_{s'} \cdots T_{s+1}T_s, \quad (\text{A.15})$$

with special cases: $T_{[s,s]} = 1 =$, $T_{[s+1,s]} = T_s$, $T_{[s,s+1]} = T_s^{-1}$ and

$$\mathbb{T}^{L_s} \equiv T_{L_s} \cdots T_3 T_2 T_1 \quad \text{and} \quad \mathbb{T}^{-L_s} \equiv T_1^{-1} T_2^{-1} T_3^{-1} \cdots T_{L_s}^{-1}. \quad (\text{A.16})$$

We also introduced the matrix: $D_5(m) = \text{Diag}[D_4(m), 1, \cdots, 1]$, where $D_4(m) \equiv \mathbb{T}^{-L_s} c_+ - c_-$,

$$D_4(m) = \frac{1+m}{2}(\mathbb{T}^{-L_s} + 1)\gamma_5 + \frac{1-m}{2}(\mathbb{T}^{-L_s} - 1) = [(\mathbb{T}^{-L_s} + 1)\gamma_5] \times \left[\frac{1+m}{2} + \frac{1-m}{2} \gamma_5 \frac{\mathbb{T}^{-L_s} - 1}{\mathbb{T}^{-L_s} + 1} \right], \quad (\text{A.17})$$

The inverses are $L^{-1}(m) = L(m)$ and

$$U^{-1} = \begin{bmatrix} 1 & T_{[1,2]} & T_{[1,3]} & \cdots & T_{[1,L_s]} \\ 0 & 1 & T_{[2,3]} & \cdots & T_{[2,L_s]} \\ 0 & 0 & 1 & \cdots & T_{[3,L_s]} \\ \vdots & \vdots & \vdots & \ddots & \vdots \\ 0 & 0 & 0 & \cdots & 1 \end{bmatrix}. \quad (\text{A.18})$$

The only non-trivial diagonal element in $D_5(m)$ can be factored

$$D_{ov}(m) \equiv D_4^{-1}(1)D_4(m) = \frac{1+m}{2} + \frac{1-m}{2} \gamma_5 \epsilon_{L_s} [\mathbb{H}], \quad (\text{A.19})$$

⁸Again we point out that the notation is a little unconventional relative to the mathematics literature, since we should really identify the “U” matrix as $\gamma_5 Q_- U Q_-^{-1} \gamma_5$, absorbing $\gamma_5 Q_-$ into the diagonal matrix.

where

$$\epsilon_{L_s}[\mathbb{H}] \equiv \frac{\mathbb{T}^{-L_s} - 1}{\mathbb{T}^{-L_s} + 1}, \quad (\text{A.20})$$

and $\mathbb{H} = (1 - \mathbb{T})/(1 + \mathbb{T})$. Gamma 5 Hermiticity requires that \mathbb{H} and therefore that \mathbb{T} is Hermitian and therefore, $T_1 T_2 T_3 \cdots T_{L_s} = T_{L_s} \cdots T_3 T_2 T_1$.

It is now straight forward to compute the matrix in Eq. 2.27

$$\mathcal{P}^\dagger \frac{1}{D_{DW}(1)} D_{DW}(m) \mathcal{P} = L(1) \text{Diag}[D_{ov}(m), 1, \cdots, 1] L(m), \quad (\text{A.21})$$

and its inverse in Eq. 2.28,

$$A = \mathcal{P}^\dagger \frac{1}{D_{DW}(m)} D_{DW}(1) \mathcal{P} = L(m) \text{Diag}[D_{ov}^{-1}(m), 1, \cdots, 1] L(1), \quad (\text{A.22})$$

where

$$A_{ss'}^{DW} = \begin{bmatrix} D_{ov}^{-1}(m) & 0 & 0 & \cdots & \cdots & \cdots & 0 \\ (1-m)\Delta_2^R D_{ov}^{-1}(m) & 1 & 0 & 0 & \cdots & \cdots & 0 \\ (1-m)\Delta_3^R D_{ov}^{-1}(m) & 0 & 1 & 0 & \cdots & \cdots & 0 \\ (1-m)\Delta_4^R D_{ov}^{-1}(m) & 0 & 0 & 1 & \cdots & \cdots & 0 \\ \vdots & \vdots & \ddots & \ddots & \ddots & \ddots & \vdots \\ (1-m)\Delta_{L_s}^R D_{ov}^{-1}(m) & 0 & \cdots & \cdots & \cdots & 0 & 1 \end{bmatrix}. \quad (\text{A.23})$$

Finally we have the crucial identity that relates the 5d and 4d determinants,

$$\text{Det}[D^{DW-1}(1)D_{DW}(m)] = \text{Det}[D_{ov}(m)], \quad (\text{A.24})$$

because the $\gamma_5 Q_- U$ factor cancels in the product and $-\text{Det}[L(1)] = -\text{Det}[L(m)] = 1$. This completes the proof that the overlap measure is equivalent to the domain wall Fermion measure with Pauli-Villars pseudo-Fermion field to give the factor $\text{Det}[D^{DW-1}(1)]$.

A.2 Domain Wall Correlators

The general bulk to bulk propagator, Eq. 2.28,

$$\langle \Psi_s \bar{\Psi}_{s'} \rangle \equiv D_{DW}^{-1}(m)_{s,s'}, \quad (\text{A.25})$$

is the domain wall inverse itself. For the Ward-Takahashi identities we need also to have boundary to bulk propagators to interior points in the domain wall. One fundamental set is

$$\langle q \bar{\Psi}_{s'} \rangle = [\mathcal{P}^\dagger D_{DW}^{-1}(m)]_{1s'} = P_- D_{1s'}^{-1DW}(m) + P_+ D_{L_s s'}^{-1DW}(m) \quad (\text{A.26})$$

$$\langle \Psi_s \bar{q} \rangle = [D_{DW}^{-1}(m) D_{DW}(1) \mathcal{P}]_{s1}. \quad (\text{A.27})$$

In addition we need bulk to bulk propagators between quark spinors

$$Q_s = [\mathcal{P}^\dagger \Psi]_s = P_- \Psi_s + P_+ \Psi_{s-1} \quad (\text{A.28})$$

and two varieties of anti-quark spinors

$$\begin{aligned} \bar{Q}_s &= [\bar{\Psi} D_{DW}(1) \mathcal{P}]_s \\ \tilde{Q}_s &= [\bar{\Psi} (-D_-) \mathcal{P}^\dagger]_s = \bar{\Psi}_s (-D_-^{(s)}) P_- + \bar{\Psi}_{s+1} (-D_-^{(s+1)}) P_+. \end{aligned} \quad (\text{A.29})$$

Thus we introduce the two correlators. The first,

$$A_{ss'}^{DW}(m) = \langle Q_s \bar{Q}_{s'} \rangle = [\mathcal{P}^\dagger \frac{1}{D_{DW}(m)} D^{DW}(1) \mathcal{P}]_{s,s'}, \quad (\text{A.30})$$

is the fundamental formula derived above. The second ‘‘mass’’ term,

$$M_{s,s'}(m) = \langle Q_s \tilde{Q}_{s'} \rangle = [\mathcal{P}^\dagger \frac{1}{D_{DW}(m)} (-D_-) \mathcal{P}^\dagger]_{s,s'}, \quad (\text{A.31})$$

is needed for the axial. There is also a very convenient factorization formula, $M(m) = A^{DW}(m)M(1)$, for this.

For the **flavor** chiral ward identity two correlators are needed

$$\begin{aligned} A_{s,1}^{DW} = \langle Q_s \bar{q} \rangle &= (1-m) X_{s-1} D_{ov}^{-1}(m) = (1-m) T_s^{-1} \dots T_{L_s}^{-1} \frac{1}{1 + \mathbb{T}^{-L_s}} D_{ov}^{-1}(m) \\ &\equiv (1-m) \Delta_s^R D_{ov}^{-1}(m). \end{aligned} \quad (\text{A.32})$$

The second one is

$$M_{1,s} = \langle q \tilde{Q}_s \rangle = \gamma_5 D_{ov}^{\dagger-1}(m) \frac{1}{1 + \mathbb{T}^{-L_s}} [T_1^{-1} \dots T_s^{-1}] \gamma_5 \equiv D_{ov}^{-1}(m) \gamma_5 \Delta_s^L \gamma_5. \quad (\text{A.33})$$

This follows from the reflection property $T_s^{-1} = T_{L_s+1-s}^{-1}$, the identity $\bar{q} = (1-m)\tilde{q} + [\bar{\Psi} D_{DW}(m) \mathcal{P}]_1$, which implies

$$M_{s,1} = \langle Q_s \tilde{q} \rangle = \Delta_s^R D_{ov}^{-1}(m) + \delta_{s,1}, \quad (\text{A.34})$$

and the fact that $\mathcal{R} D_-^{-1} D^{DW}(m)$ is γ_5 Hermitian, so that $\langle q \tilde{Q}_s \rangle = \gamma_5 \mathcal{R}_{ss'} \langle Q_{s'} \tilde{q} \rangle^\dagger \gamma_5$.

Finally for the chiral anomaly in the **singlet** current, we need the correlator

$$\begin{aligned} M_{ss'}(m) &= \langle Q_s \tilde{Q}_{s'} \rangle = A_{ss''}^{DW}(m) M_{s'',s'}(1) = (1-m) \Delta_s^R D_{ov}^{-1}(m) M_{1,s'}(1) + M_{s,s'}(1) \\ &= (1-m) \Delta_s^R D_{ov}^{-1}(m) \gamma_5 \Delta_{s'}^L \gamma_5 + M_{s,s'}(1), \end{aligned} \quad (\text{A.35})$$

for the anomaly with $s = L_s/2 + 1$, $s' = L_s/2$.